Three-dimensional graphoepitaxial growth of oxide films by pulsed laser deposition

Peter B. Mozhaev* and Julia E. Mozhaeva
Institute of Physics and Technology of the Russian Academy of Sciences, Moscow, 117218, Russia

Alexey V. Khoryushin, Jørn Bindslev Hansen, and Claus S. Jacobsen
Department of Physics, Technical University of Denmark, Kongens Lyngby, DK-2800, Denmark

Igor K. Bdikin
TEMA-NRD, Mechanical Engineering Department and Aveiro Institute of Nanotechnology (AIN), University of Aveiro, Aveiro, 3810-193, Portugal

Iosif M. Kotelyanskii and Valery A. Luzanov
Kotelnikov Institute of Radioengineering and Electronics of Russian Academy of Sciences, Moscow, 125009, Russia

(Received 3 August 2018; published 9 October 2018)

Metaloxide thin films were deposited on tilted-axes $NdGaO_3$ substrates (TAS NGO) by pulsed laser deposition. A specific growth mode resulting in an inclination between crystallographic planes of the top layer and that of the bottom layer was commonly observed. A simple geometrical growth model, taking into account faceting of the surface of the bottom layer, explains the observed dependencies well. The matching of the top and the bottom layer is essentially three dimensional, with graphoepitaxial matching in the substrate plane. The three-dimensional graphoepitaxial (3DGE) growth mechanism seems to be quite common for deposition on TAS with tilt angles more than 5°. It was observed for eight of ten studied combinations of materials, including multilayer heterostructures, for four different deposition techniques, and on substrates with different predeposition treatment. The 3DGE growth was observed both with increase and decrease of the top layer tilt angle compared to the tilt angle of the bottom layer. Two different 3DGE dependencies can be distinguished in the high-angle range (>15°): with a tendency towards standard growth above some threshold angle, and retaining 3DGE behavior until a tilt angle of 45° is reached, either by the top or by the bottom layer. In a simplified way the difference may be attributed to two different formation mechanisms: the first one generates the additional tilt when the growing grain overgrows another grain, seeded on the next step on the substrate surface, while for the second mechanism the inclination is formed when the grain is seeded over the step. The first type is better described by a tangent angular dependence, it is observed usually when a compressive strain is induced in the top layer. The second type follows a sine dependence, and is usually seen for a tensile-strained top layer.

DOI: 10.1103/PhysRevMaterials.2.103401

I. INTRODUCTION

Deposition of epitaxial thin oxide films on substrates with inclination of surface orientation from the small-index crystallographic planes (SICPs)—the tilted-axes substrates (TAS), often also called "miscut" or "vicinal" substrates—is attracting more and more attention in the last decades as a simple way of preparation of quantum wires and quantum dots (see, e.g., [1]). Previously studies of oxide films deposition on TAS was usually pursuing the goal of improvement of the lattice perfection and surface smoothness due to change of the growth mechanism from 3D (Vollmer-Weber or Stransky-Krastanov modes) to the two-dimensional (2D) step-flow growth (see, for example, [2–4]). The reason for such a change is the surface structure of the TAS, representing a network of steps with terrace and edge surfaces oriented along the SICPs (see, e.g., [5]). The SICPs forming the terraces for some substrate materials and orientations are called "habit planes," because the standard deposition on these materials is done with substrate surface orientation along the "habit" SICP. This network of steps provides excellent seeding positions in the internal corners formed by the step edge and the surface of the next terrace, and force the unidirectional growth from the edge of the terrace [Fig. 1(a)]. The overgrowth of the grain seeded on the next joint of terrace and edge determines the general properties of the growing film: strain, orientation, dislocations density, and surface roughness. Note that the strain in the overgrowth area is generated not only by the in-plane mismatch due to the difference of the lattice constants of the film and the substrate, but also by the out-of-plane mismatch [not shown in Fig. 1(a)]. This "standard" growth mode [Fig. 1(a)] demonstrates good parallelism of crystallographic planes of the film and the substrate, and the strain, generated by the film-substrate lattice mismatch, is accommodated by generation of dislocations and step bunching (see, e.g., modeling in [6]). Some authors even claim this standard growth mechanism with parallel SICPs of the film and the substrate to be the only possibility.

*Corresponding author: pbmozh@gmail.com

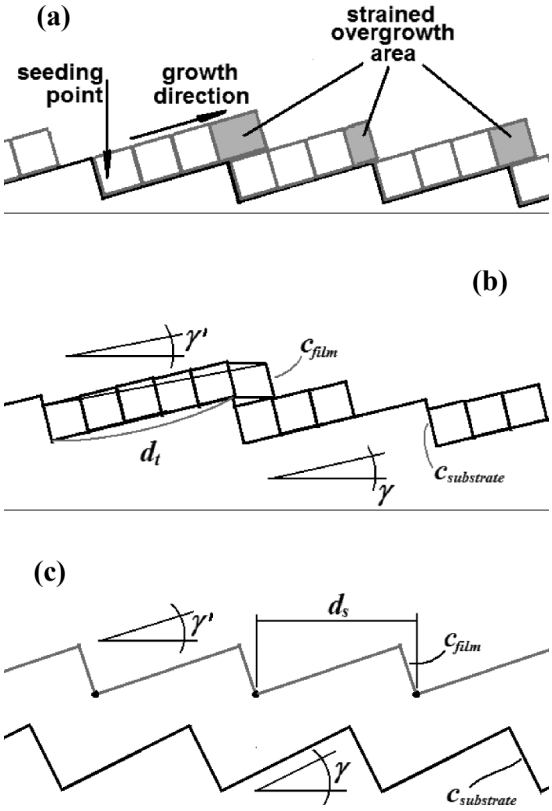

FIG. 1. Growth modes during oxide deposition on tilted-axes substrates: (a) Standard growth mode with parallel small-index crystallographic planes (SICPs) of film and substrate. (b) and (c) Three-dimensional graphoepitaxial growth mode with mutual inclination of film and substrate planes. (b) Overgrowth mechanism, when inclination between the SICPs of the substrate and the film is caused by a difference between the height of the substrate step and the layer thickness of the film on the next terrace. The case of smaller height of the growth step of the film is shown. The resulting tilt follows the tangent formula [Eq. (1) in text]. (c) Simultaneous seeding of the film on neighboring seeding knots (black dots) results in the sine model [Eq. (2)].

In fact, studies of deposition of semiconducting thin films on TAS showed the possibility of different film-substrate orientational relations, depending on the mechanism of lattice-mismatch strain accommodation. The first observations of inclination of the SICPs of the film from that of the substrate date back to the early 1970s [7–10]. The mechanisms resulting in such inclinations were discussed in different ways in [11–13]. According to [13], three epitaxial modes are possible, with lattice mismatch accommodation by (i) dislocations with Burgers vector in the habit plane, (ii) dislocations with Burgers vector inclined relative to the habit plane, and (iii) disconnections generated on the edges of the terraces on the TAS surface. The first mode corresponds to the standard mode [Fig. 1(a)], with no inclination of the SICPs of the film from that of the substrate, and with the lattice-mismatch generated strain being completely relaxed by generation of dislocations. The second mode results in some (usually small) inclination of the lattice of the crystallites of the growing film, it is usually detected as an increased width of the out-of-substrate plane rocking curve of the film compared to the corresponding rocking curve of the substrate. The inclination mainly depends on the mismatch between the substrate and film, and for deposition on a substrate aligned along a SICP (habit plane) the crystallites are inclined randomly, or almost randomly, in the substrate plane. Systematic small-angle (usually below 1°) tilt of the films SICP along some crystallographic direction in the substrate plane also manifests this second relaxation mechanism (see, e.g., [14]). The third epitaxial mode is a result of accommodation of strain by disconnections generated on the edges of the steps. The inclination of the film lattice depends on both lattice mismatch and substrate plane tilt from the habit plane and may be described in a simple geometric way first proposed by Nagai [8]. The height of the growth steps of the film c_f [Fig. 1(b)] is not equal to the height of the steps on the substrate surface c_s. As a consequence, the inclination of the crystallographic planes of the film from the substrate surface plane γ' increases compared to the substrate tilt γ when $c_f > c_s$, and decreases when $c_f < c_s$. Considering overgrowth of the layers (see, e.g., [15]) with average length of the terrace surfaces d_t [Fig. 1(b)], we can write the obvious relations

$$d_t = c_f/\tan\gamma' = c_s/\tan\gamma,$$
$$\gamma' = \arctan[(c_f/c_s)\tan\gamma]. \quad (1)$$

This simple formula may change if seeding is considered not in a single edge-terrace joint, but simultaneously on neighboring seeding knots (black dots in Fig. 1(c), [16]). In this case simple considerations provide the sine dependence instead of tangent:

$$d_s = c_f/\sin\gamma' = c_s/\sin\gamma,$$
$$\gamma' = \arcsin[(c_f/c_s)\sin\gamma], \quad (2)$$

where d_s is the average distance between the seeding knots on the substrate surface. Usually the authors do not distinguish the two possible mechanisms and use sine or tangent for their convenience, or even ignore the trigonometric functions and calculate the angle directly. The reason is the *vicinal* range of the tilt angles, in most of the studies less than 5° and only in some studies increasing to ∼10°.

It is important to note that c_f and c_s are not the lattice constants, but the heights of the steps of film and substrate, only in some cases being equal to the lattice constants of the materials in respective directions (normal to the corresponding habit plane). For example, the height of step can be 1/2 or 1/3 of the lattice constant ([17] and [15], correspondingly), or a fractional part of the translation distance in the cases when faceting happens along (110) or (111) SICPs.

This epitaxial growth mode is essentially three dimensional: the tilt axis of the substrate provides initial bonding conditions for the film, usually similar to the epitaxial relations on the habit plane, while the translation distance (d_t or d_s) and the ratio of substrate to film step heights determines the mutual orientation of the habit plane of the substrate and the corresponding SICP of the film. The film and the substrate are coupled, thus, in all three dimensions, while for ordinary epitaxial growth the coupling occurs only in the substrate plane, i.e., in two dimensions. At the same time, this growth mechanism may be considered as a kind of graphoepitaxy,

because the orientation and structure of the film is determined not exclusively by ions in the lattices of film and substrate, but also by a net of features on the substrate surface with the size greater than the interatomic distances or lattice constants. To indicate all these features we will refer to this growth mechanism as the three-dimensional graphoepitaxial (3DGE) growth mode.

The three mechanisms of mismatch relaxation may coincide, with corresponding change of inclination angle and strain to some intermediate values between the pure cases [13].

The 3DGE mechanism, fairly described with geometrical approximation, was observed in numerous studies of semiconductor heteroepitaxy, references can be found in [11–13]. Most of these heterostructures were limited to small tilt angles (vicinal range), utilized in semiconductor technology for improvement of thin film quality. Oxide thin films and substrates were rarely studied and most of the obtained tilts in oxide heterostructures were misinterpreted or left without explanation.

To our knowledge, 3DGE in all-oxide heterostructures was first observed in 1991 by Kotelyanskii and Luzanov [18], when CeO_2 films were deposited on $NdGaO_3$ (NGO) TAS (tilt around the [001] axis from the (110) plane towards (010) plane) with e-beam evaporation. All range from (110) to $(-1\ 1\ 0)$ planes [orthorhombic notation, equivalent to the $(100)_c$ and $(010)_c$ planes of the pseudocubic notation for the NGO crystal] was studied. The $\langle 110\rangle$ axis of the CeO_2 film was bound to the [001] tilt axis of the substrate for all TAS orientations. The inclination of the CeO_2 (001) SICP from the sample surface monotonously increased surpassing the increase of the substrate tilt angle, until (110) CeO_2 orientation was reached at $\gamma_c \approx 32^\circ$ [Fig. 2(a), solid line]. The faster increase of film tilt γ' compared to the substrate tilt γ was due to greater lattice constant of the film (5.4 and 3.86 Å, correspondingly), and showed good agreement with the simple formula (2). The film remained (110) oriented with a wide spread of grains orientation (rocking curve width $\sim 5^\circ$) until $\sim 58^\circ$ substrate tilt, when 3DGE started to follow the $(-1\ 1\ 0)$ crystallographic plane of the substrate, symmetrically equivalent to the initial (110) NGO plane. The reason for (110)-oriented film growth is the presence of two symmetrically equivalent {110} SICPs on the substrate surface, each of them showing no preference over the other neither in the resulting tilt of the film, nor in the area of the corresponding facets on the substrate surface. The critical tilt angle at which the growth mode changes from 3DGE to (110) oriented is given by simple formula [sine dependence of tilt (2)]

$$\gamma_c = \arcsin[(c_s/c_f)\sin(45^\circ)]. \tag{3}$$

For CeO_2 deposition on NGO $\gamma_c \approx 30.4^\circ$, in a reasonable agreement with the observed value.

The study of CeO_2/NGO heterostructures was continued using rf sputtering [19,20] and pulsed laser deposition (PLD) techniques [16,21]. Much higher deposition rate during rf sputtering (5–7 nm/min instead of 0.5 nm/min for e-beam evaporation) resulted in a more complicated behavior [19,20]. Both standard growth mode (type I in [19,20]) and 3DGE

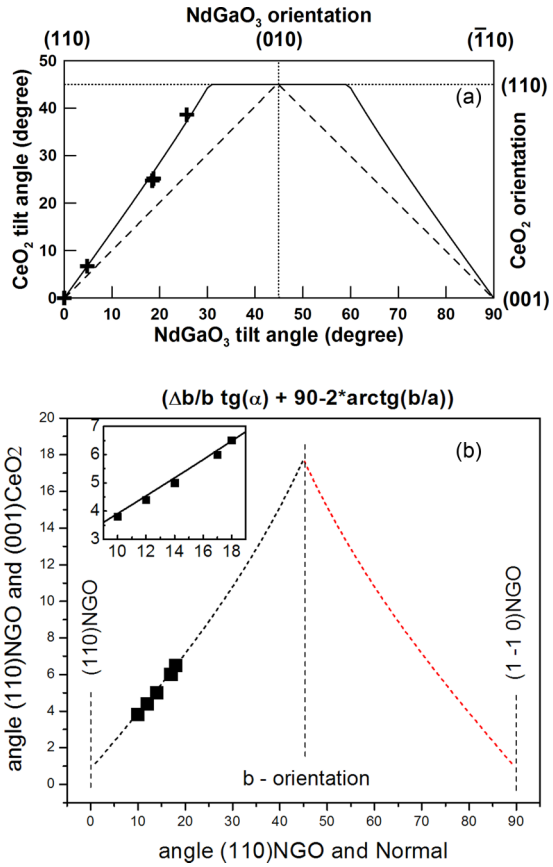

FIG. 2. First observations of gradual increase in tilt of crystallographic planes of the film in CeO_2 deposition on $NdGaO_3$ tilted-axes substrates. (a) With e-beam evaporation (solid line, [18]) and rf sputtering (crosses, [19,20]). The tilt of CeO_2 film with standard epitaxial growth mode is shown by a dashed line. (b) With PLD [22]. The formula on the graph takes into account the orthorhombicity of $NdGaO_3$. Note that dependencies follow the sine formula [Eq. (1)] for (a) and the tangent formula [Eq. (2)] for (b).

growth mode (type II) are degenerated twice due to the presence of symmetrically equivalent (110) and $(-1\ 1\ 0)$ planes on the substrate surface. The angular dependence of the 3DGE part of the film followed the same sine mode (2) as for e-beam evaporation [Fig. 2(a), crosses]. Further increase of the deposition rate for PLD (7–55 nm/min average deposition rate, depending on the laser repetition rate, and above 100 nm/min peak deposition rate during the laser pulse) provided 3DGE growth in the 4°–20° substrate tilt angle range [21]. At higher angles the inclination between the NGO (110) plane and the CeO_2 (001) plane dropped to 2°–3° and remained at this level over the range ($23^\circ < \gamma < 30^\circ$). Formula (1) was applied to the 3DGE growth during PLD in [16] [Fig. 2(b)] and showed excellent agreement with the observed mutual film and substrate orientation. The more complicated view of the formula in Fig. 2(b) compared to formula (1) is due to an attempt to take into account the orthorhombic structure of the substrate; in fact, this correction is small and may be neglected. Deposition of $YBa_2Cu_3O_x$ (YBCO) over the CeO_2 layer on NGO TAS resulted in a similar linear increase of the

film inclination and abrupt drop to $\sim 2.5^\circ$ when γ exceeded 25° [21].

PLD of CeO_2 buffer layer on Ni biaxially textured tape with grain orientations randomly spread from the substrate surface plane was studied in [17]. At high deposition temperatures the out-of-substrate plane tilt of the (001) plane of the CeO_2 overlayer follows the tilt of the (001) plane of the Ni grain below, but is smaller, in a qualitative agreement with the geometric formula. At low deposition temperature the crystallites of CeO_2 are smaller than the terrace width on the Ni grain surface; this excludes the graphoepitaxial effect of steps on the film orientation, and, in fact, the CeO_2 film grows in an agreement with the standard growth mode, $(001)CeO_2||(001)Ni$ [17]. Authors mention that grains of $LaMnO_3$ and Y-stabilized ZrO_2 (YSZ) also tilted according to the geometrical model when deposited on Ni tapes [17].

Similarly, in [15] another fluorite material, YSZ, deposited on the vicinal sapphire substrate [5° from (0001) plane] with liquid phase epitaxy (LPE), showed mixed orientation from the standard growth mode to the 3DGE growth mode. The reason was intense step bunching on the substrate surface during substrate preparation (annealing at 1500 °C), resulting in broad (0001)-oriented terraces. Some of the YSZ crystallites were small enough to fit one terrace, and showed orientation $(001)YSZ||(0001)Al_2O_3$, while orientation of the big YSZ grains showed a tilt of 5.9°, in an excellent agreement with the geometrical model [15].

YBCO deposition by PLD on YSZ TAS and CeO_2-buffered sapphire TAS was demonstrated in [22]. Both cases showed 3DGE, assuming that the CeO_2 buffer layer is well oriented along the sapphire SICP : $(001)CeO_2||(1\ -1\ 0\ 2)\,Al_2O_3$. We will discuss the results of [22] in more detail in the Discussion section below.

YBCO deposition on YSZ TAS was also studied in [23]. Direct deposition resulted in *c*-oriented YBCO films independent of the substrate tilt angle, but introduction of a buffer Y_2O_3 layer between YBCO and YSZ blocked chemical interaction and promoted film growth with a tilt of SICP. The inclination of the YBCO film from the habit plane shows the 3DGE behavior (increase of the inclination with an increase of the substrate tilt angle), but the measured value of the film tilt is less than calculated using the simple formula (1). At high substrate tilt angle (35.7°) the YBCO film grows in the standard epitaxial mode with small (less than 1°) deviation from the habit plane (001) YSZ [23].

$PbTiO_3$ deposition on $SrTiO_3$ TAS [24] showed good agreement with the geometrical model, even though the mechanism of growth is much more complicated than in other discussed studies (*a*-oriented grains formation on the edges of the steps, with corresponding strains and distortions introduced into the *c*-oriented grains on the terraces). Another study of $PbTiO_3$ deposition on TAS, with MgO substrates [25], also resulted in the growth similar to the 3DGE, but with higher inclination of the film compared to the calculated using the table data.

Summarizing, the 3DGE growth mode is not something unusual for all-oxide heterostructures on TAS, but the mechanism was quite often not recognized, and the results were misinterpreted. Systematic investigations of the growth mode are lacking, the angular ranges of 3DGE growth were not determined. Deviations from the simple geometrical formula were not explained. At the same time, understanding of the 3DGE mechanism is important for the fabrication of thin film heterostructures, especially when the materials are highly anisotropic, like high-temperature superconductors (HTSC) or piezoelectrics.

In this paper we present our observations of the 3DGE growth in different film-substrate pairs. Preservation of the 3DGE growth mode through a multilayer system is demonstrated, and the characteristic features of the growth mode and deviations from the simple geometrical model are discussed. In this study we will concentrate on orientational characteristics of the 3DGE films and multilayers, the fabrication detail and secondary growth features will be presented in another publication.

II. EXPERIMENTAL TECHNIQUES

The TAS ($5 \times 5 \times 0.5\,mm^3$) were cut from $NdGaO_3$ single crystals, their substrate surface was set by tilting from the (110) habit plane around the [001] axis towards the (010) plane (corresponding to tilt around the $[001]_c$ axis from the $(100)_c$ plane towards the $(-1\ 1\ 0)_c$ plane in the pseudocubic notation). The nominal tilt angle varied in the range 0°–34°. Chemical-mechanical polishing (CMP) of the substrates provided atomically flat surfaces with a roughness R_a determined by atomic force microscopy (AFM) below 2 Å. Such a low roughness implies presence of a damaged "amorphous" layer on the surface of the substrate after CMP. Formation of pronounced steps on the surface with terraces and edges oriented along the {110} planes (surface recrystallization) demanded additional treatment: wet etching with HF and high-temperature annealing in oxygen (to be published). Mainly depositions were done on the as-polished substrates, only after rigorous cleaning in organic solvents and weak acid to remove contaminants present after dicing and CMP. The actual tilt orientation and angle of the substrate surface were checked after CMP with XRD measurements. The deviation of the actual tilt axis from the [001] axis of $NdGaO_3$ did not exceed 5°, being usually less than 2°. The actual tilt angle was measured for each substrate.

Fluorite YSZ and CeO_2, perovskite $BaZrO_3$ (BZO), and perovskitelike YBCO thin films were deposited in different combinations with PLD. The details of the technique can be found in [26]. Commercially available stoichiometric high-density (>90% of bulk density) ceramic targets were used. The structural properties of thin films and multilayers were studied using x-ray diffraction techniques, the surface morphology was observed by SEM and AFM. Electrical properties of the superconducting films were measured with noncontact techniques. The complete results of our studies, including morphology and electrical properties of the films, will be published elsewhere: in this article we will concentrate only on the orientational features of the heterostructures.

The chosen film and substrate materials provided a wide range of lattice mismatch and corresponding strain introduced into the upper layer. The translation distances at room temperature and expected strain in the habit plane (110) NGO are presented in Table I for all studied top layer/bottom layer combinations. The lattice mismatches, in fact, differ from the

TABLE I. Lattice parameters of the substrate and film materials.

Top layer			Calculated in-plane strain[a] (%)			
Bottom layer	Translation distances[b] (Å)		Y : ZrO_2	CeO_2	$BaZrO_3$	$YBa_2Cu_3O_x$
	in-plane	out-of-plane				
$NdGaO_3$ Orthorhombic	3.861 × 3.864[c]	3.861	+5.7– + 5.8	+1.0– + 1.1	−8.7– − 8.8	−0.75– + 1.0
Y : ZrO_2 Cubic	3.641[d]	5.149	xxx	−5.0	−15.4	−6.8– − 5.1
CeO_2 Cubic	3.822[d]	5.405		xxx		−1.8– − 0.1
$BaZrO_3$ Cubic	4.20	4.20			xxx	+7.4– + 8.9
$YBa_2Cu_3O_x$ Orthorhombic	3.825 × 3.89	3.89–3.92[e]				xxx

[a]Negative value corresponds to compressive strain, positive to tensile strain.
[b]"In-plane" data are provided for the standard (110) orientation of the NGO substrate and corresponding SICPs of the films. Lattice structure and parameters are given for room temperature.
[c]Orthorhombic lattice of $NdGaO_3$ results in orthogonal translation directions on the (110) plane with distances $c/2 = 3.864$ Å and $[(a^2 + b^2)^{1/2}]/2 = 3.861$ Å.
[d]Fluorite lattice during deposition on perovskite $NdGaO_3$ substrate is tilted in substrate plane by 45° and the in-plane translation distances corresponding to the substrate axes are calculated as $5.149/2^{1/2} = 3.641$ and $5.405/2^{1/2} = 3.822$ Å for YSZ and CeO_2, respectively.
[e]Perovskitelike lattice of YBCO consists of three perovskite cells in *c* direction, so the out-of-plane translation distance is given by $c/3 =$ 3.89–3.92 Å, depending on the oxygen contents in the film.

presented, as a result of different thermal expansion coefficients, but since the lattices of both layers can be distorted by the substrate-induced strain, by presence of oxygen vacancies, and by chemical interaction between layers, we cannot present exact values of the strain and keep the room-temperature data as a reference. Actual strain should be determined for each top layer/bottom layer combination using the measured lattice constants in the fabricated heterostructures.

The deposition parameters for CeO_2 and YSZ were optimized to obtain smooth thin films of single orientation $(001)CeO_2||(110)$ NGO on a standard (110) NGO substrate. Substrate temperature during deposition was held at 740 °C, the target was ablated at an energy density of 1.1 J/cm^2 and pulse repetition rate of 2 Hz in a mixture of argon and oxygen (6% O_2, 0.2 mbar total pressure). Low energy density just above the ablation threshold (∼1 J/cm^2 in our deposition system) resulted in a very low growth rate (∼0.3 Å/pulse = 0.6 Å/s for CeO_2 and ∼0.1 Å/pulse = 0.2 Å/s for YSZ), and low oxygen partial pressure promoted growth of a film of high crystal quality. No post-deposition annealing was performed; the film was cooled down to room temperature in the working atmosphere at the maximal possible rate.

The lattice constant of the YSZ films on (110) NGO substrates was typically 5.145–5.155 Å, for some samples ranging from 5.135 to 5.185 Å, in good agreement with standard value of 5.15 Å. The FWHM (full width at half maxima) of the peaks on the $\theta/2\theta$ scans for the YSZ films was very close to the estimations of the size broadening, implying high homogeneity and low strain in the films. The CeO_2 films on (110) NGO substrates showed lattice constant 5.395–5.41 Å, close to the standard 5.4 Å. The FWHM of the peaks on the $\theta/2\theta$ scans was significantly higher than the size broadening, indicating strained or inhomogeneous layer formation. Both YSZ and CeO_2 films showed wide rocking curves (see Table II).

TABLE II. Typical structural properties of the films grown in standard epitaxial mode on low-angle TAS NGO. The spread of the presented parameters is ∼50%. Actual film properties strongly depend on deposition conditions.

Film/substrate	Lattice mismatch[a] (%)	Lattice constant[b] (Å)	Strain $\Delta d/d$ (%)	FWHM of rocking curve (deg)	Film SICP inclination (deg)	Vicinal range (deg)
YSZ/NGO	+5.7– + 5.8	5.149	0.25	1.1	<0.5	2
CeO_2/NGO	+1.0– + 1.1	5.405	0.15	0.5	<0.15	1
$YBa_2Cu_3O_x/CeO_2$	− 0.75– + 1.0	11.685	0.4	0.35	<0.1	1
$BaZrO_3$/NGO	− 8.7– − 8.8	4.200	0.6	0.5	<0.1	no data

[a]Negative value corresponds to compressive strain, positive to tensile strain.
[b]Normal to substrate plane.

BZO films were deposited at the same conditions as fluorite films. The deposition rate for BZO was 0.225 Å/pulse = 0.45 Å/s. The BZO films showed good lattice perfection as determined by XRD $\theta/2\theta$ scans and rocking curves (Table II). The lattice constant was 4.197–4.213 Å, in good agreement with the bulk value ($\sim$ 4.2 Å).

The YBCO thin films deposition parameters (1.2–1.5 J/cm^2, oxygen partial pressure 0.16 mbar, total pressure of Ar/O_2 mixture 0.8 mbar) were optimized to obtain the best superconducting and structural properties for the films grown on the standard (110) NGO substrates. Relatively low deposition temperature of 730–750 °C suppressed the chemical interaction of YBCO with CeO_2 bottom layer in multilayer structures. The deposition rate of 0.8 Å/pulse (1.6 Å/s at standard 2 Hz laser pulse repetition rate) provided enough time for relaxation of the deposited material on the surface of the growing film. A prebake step before deposition saturated the substrate surface with oxygen and decreased the probability of chemical interaction with the growing film. As a consequence, the lattice perfection of the film significantly increased, especially for the thin layer near the interface with the substrate [26], and both size and density of the particles on the thin film surface decreased. Post-deposition annealing was performed at 450 °C in 800 mbar of oxygen for 1 h. All YBCO films showed T_c above 89 K and a narrow superconducting transition, proving good uniformity of the film structure. The c lattice constant for all films was 11.67–11.7 Å, confirming good reproducibility of the film fabrication procedure. Rocking curve width, FWHM of the peaks of the $\theta/2\theta$ scans, and strain estimation, depended on tilt angle, underlying material, and deposition conditions, and varied significantly.

Multilayers were usually prepared *ex situ* to have a possibility to study the bottom layer properties before and after deposition of the top layer. Some multilayer structures were fabricated *in situ*, their parameters were compared with that of corresponding *ex situ* fabricated heterostructures.

Deposition rate of the deposited materials was calibrated using selective wet chemical etching of grown films or with lift-off removal of some part of the fabricated layer using a predeposited and patterned hard mask. The value calculated using a number of pulses on target and calibrated deposition rate we call the *nominal* thickness. Actual film thickness may differ from the nominal value not only as a result of small deviations of deposition parameters, but also due to modification of the target surface by laser irradiation, usually resulting in a lower ablation rate with time. The thickness was also evaluated using the Williamson-Hall method, the result was in good agreement with the nominal value (error below 15%). Application of the Williamson-Hall calculation allowed also determination of the variation of the diffraction period normal to the diffraction plane $\Delta d/d$. This parameter, usually called "strain," was determined for films of all materials if more than one diffraction peak was present on the $\theta/2\theta$ scan. Note that this is not the strain related to the film-substrate lattice mismatch (Table I), though sometimes a relation can be established between these two parameters.

III. RESULTS

The studies of epitaxial growth in semiconductor heterostructures showed that the tilt axis acts as an anchor setting the initial epitaxial relation along the habit plane. Similarly, in our previous studies [19–21] the ⟨100⟩ axes of the perovskite films and the ⟨110⟩ axes of the fluorite films were parallel to the substrate tilt axis [001] NGO for all deposition conditions. In this study we assumed that this epitaxial relation remains correct and limited the XRD studies to $\theta/2\theta$ and ω scans around the substrate tilt axis with an initial offset angle ω_0. Our assumption is corroborated by similar integral intensity of the XRD peaks for the films with the same nominal thickness. When the observed peak integral intensity was significantly smaller, we performed a search for additional orientations. All orientations found still followed the same epitaxial relation with some of the film axes parallel to the substrate tilt axis.

To avoid misunderstanding we will use the following notations:

(i) the substrate plane is the plane of substrate surface;

(ii) the tilt angle γ is the angle between the SICP of film or substrate (habit plane) and the substrate plane;

(iii) the inclination angle is the angle between the SICPs of the substrate and the film;

(iv) the misorientation is the spread of orientations of individual grains of the film around the main orientation, usually determined as FWHM of the corresponding rocking curve.

A. Standard epitaxial growth

The epitaxial growth for very small tilt angles (vicinal range) does not differ much from growth on a substrate ideally oriented along the habit plane. In fact, the surface of a substrate exactly oriented along the habit plane usually consists of local areas with very small tilt from the habit plane: only the average orientation corresponds to the SICP (see, for example, discussion of different effects of roughness in [11]). In our case morphological, structural, and electrical parameters of the films remain the same as for the (110) NGO substrate until some threshold tilt value; this angle determines the vicinal range of epitaxy. Usually in this range the tilt of the film due to the 3DGE growth hardly can be distinguished from the tilt due to other mechanisms, taking into account the accuracy of the XRD measurement and relatively high misorientation of the film grains after PLD. Morphologically the surface of the film shows no specific directions and the grains are rounded or evenly oriented, if elongated.

At the same time, the films obtained in the vicinal range with the "standard" epitaxial growth mode may be considered as a reference for the 3DGE grown films at higher tilt angles. For this reason in this section we present the main parameters of all films deposited on TAS of the vicinal range (see Table II).

Generally we note that the parameters of the films grown in the vicinal range depend on conformity of the lattice structure and the mismatch strain introduced by the substrate. The fluorite films deposited on the perovskite substrates show a wider rocking curve and higher deviation of the average orientation from the (110) NGO plane compared with the perovskite films, but much lower variation of the out-of-plane

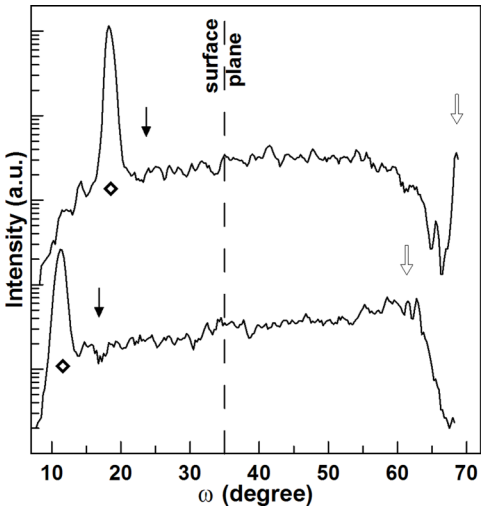

FIG. 3. Rocking curves for the (400) peak of CeO_2 films on TAS NGO. Substrate tilt angle: top curve 11.4°, bottom curve 18.4°. Black arrows show the angular position of the (110) NGO plane, white arrows correspond to the angular position of the (010) NGO plane. The 3DGE peaks of CeO_2 films are marked with diamonds.

lattice constant $\Delta d/d$. Both for fluorite and perovskite films the structural parameters are better for the materials with smaller lattice mismatch.

Deposition of YBCO on NGO TAS in all conditions and for all tilt angles resulted in standard epitaxial growth with relations ⟨100⟩ (001) YBCO||[001](110) NGO. The details of these films structure, morphology, and superconducting properties can be found in [21,27]. Such preservation of standard growth mode on TAS of all angles is considered as usual for YBCO deposition on perovskite substrates (see, e.g., [3], and [19–21,27]).

In our previous studies we assumed that a difference in the lattice structure is an important condition of 3DGE growth: a perovskite film on a perovskite substrate (like YBCO on NGO) and a fluorite film on a fluorite underlying layer would follow standard epitaxial growth mode. In fact, this is not true, as we will show below.

B. 3DGE growth

1. CeO_2 on NGO TAS

Typical rocking curves of CeO_2 films deposited by PLD on TAS NGO are presented in Fig. 3. The 3DGE peak is shifted from the position of the (110) NGO plane towards higher tilt angles, and the shift increases with substrate tilt angle. All our results for 3DGE growth of CeO_2 at different substrate tilt angles are gathered in Fig. 4(a). The film orientation dependence on substrate tilt is finely described by the simple geometrical model (1) until ∼20°. Above this value the film tilt decreases towards the standard epitaxial relation (001) CeO_2||(110) NGO. For substrate tilt angles 30°–35° we observed (110)-oriented CeO_2 films, with wide rocking curves (up to 4°) and high strain ($\Delta d/d \approx 1°$). These results are in good agreement with [18] and limitations of the simple geometrical model (3). Detailed description of deposition technique, (110)-oriented CeO_2 films properties, and specific cases in the angular range 30°–45°, will be presented in another publication. The CeO_2 film orientation for the tilt angles 25°–30° remains unclear: we could not reliably detect weak high-index XRD peaks from the CeO_2 film. Formation of a polycrystalline film seems probable, maybe with a set of predominant orientations.

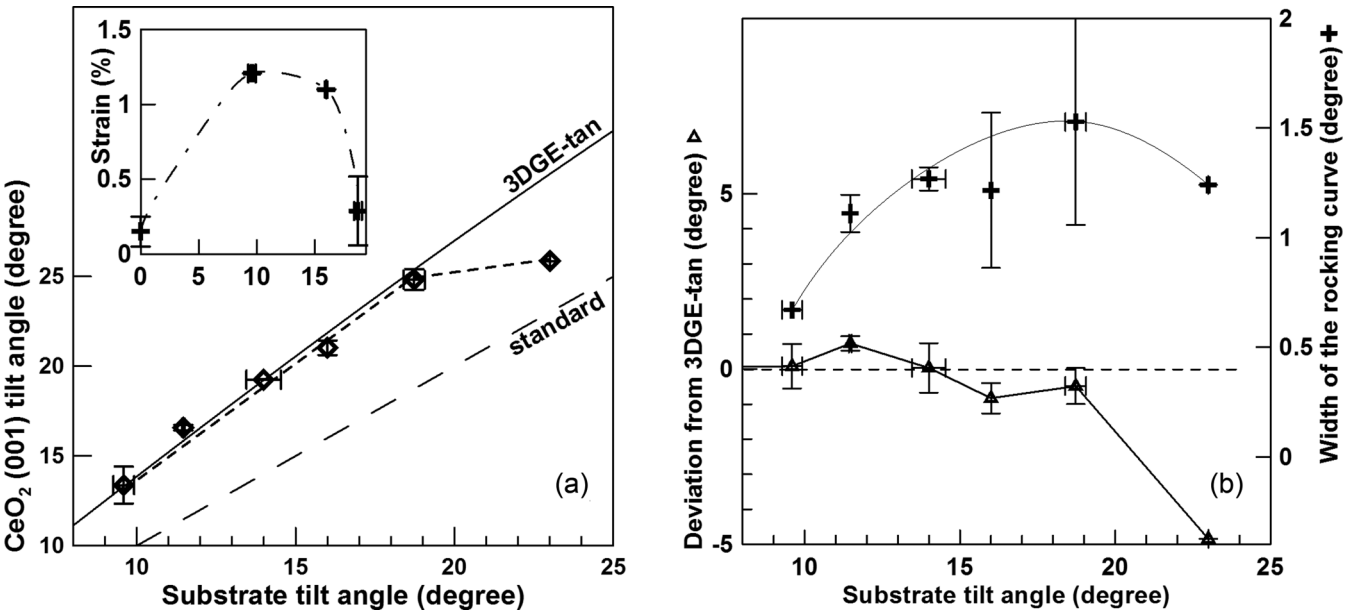

FIG. 4. Orientational relations of CeO_2 films on TAS NGO. (a) The film orientation follows the 3DGE-tangent growth mode [Eq. (1)] until 20°, and then the film tilt deviates towards the standard growth mode. Inset: Dependence of the lattice constant variation (strain) on the substrate tilt angle. (b) Deviation from calculated tilt angle (triangles) changes from small positive to small negative with substrate tilt angle until threshold at 20°. The width of rocking curve (crosses) increases with angle. Lines are given as guides for the eye.

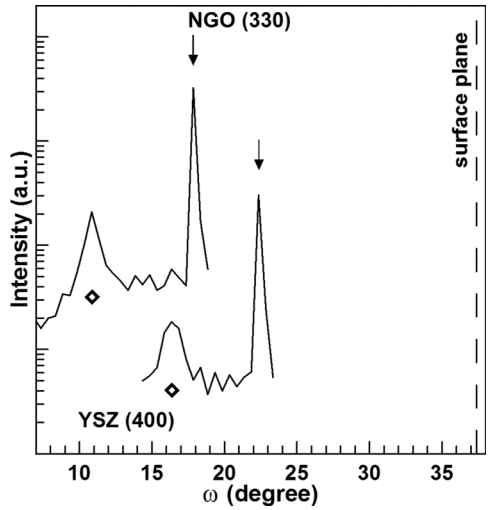

FIG. 5. Rocking curves for the (400) peak of the YSZ films on TAS NGO. Substrate tilt angle: top curve 19.5°, bottom curve 15.4°. Arrows show the angular position of the (110) NGO plane, the 3DGE (400) YSZ peaks are marked with diamonds.

The deviation of the film orientation from the calculated value depends on film properties and deposition parameters. On average, the 3DGE film shows tilt angle slightly ($<1°$) higher than calculated for tilt angles below 14°, and slightly ($<1°$) smaller for tilt angles above this threshold, with a rapid increase of deviation when the film stops following pure-3DGE growth mode for tilt above 20° [Fig. 4(b)].

The misorientation of CeO_2 grains was tested using the XRD rocking curves measurements. For an increase of γ from 0° to 19° the FWHM of the rocking curves, as well as spread of the FHWM's from sample to sample, increased [see Fig. 4(b), top curve]. When the growth mechanism turns towards the standard mode ($\gamma = 23°$), the width of the rocking curve decreases.

The lattice constant of the CeO_2 3DGE films on TAS is close to that of the films on (110) NGO substrate, 5.399–5.408 Å. The strain and the FWHM of the rocking curves for the majority of the 3DGE films are significantly higher (∼1% and ∼1.3°) than that of the standard films (∼0.15% and ∼0.5°, see Table II). The FWHM of the peaks on the $\theta/2\theta$ scans is higher than expected on the size evaluation, implying significant inhomogeneity of the films similarly to the standard-oriented films grown on (110) NGO. Small deviations from optimal deposition conditions influences the 3DGE films properties in the same way as that of the standard films: the lattice constant increased and the strain in the film decreased with a decrease of the oxygen partial pressure during deposition. The rocking curve width showed no dependence on deposition conditions in the studied range.

2. *YSZ on NGO TAS*

The typical rocking curves of the YSZ thin films on TAS NGO are shown in Fig. 5. The Bragg diffraction angle for the (400) peak of YSZ is very close to that of the (330) peak of the NGO substrate, so a single measurement allows determination of angular positions of both substrate and film SICPs.

Typical dependence of the YSZ film orientation on substrate tilt angle is shown in Fig. 6(a). The tilt of the (100) plane of YSZ follows the geometrical model, sine variant (2), exceeding the calculated value in the angular range 5°–12°. The deviation from the 3DGE model is much higher than for CeO_2 3DGE films, reaching +3° for substrate tilt angles

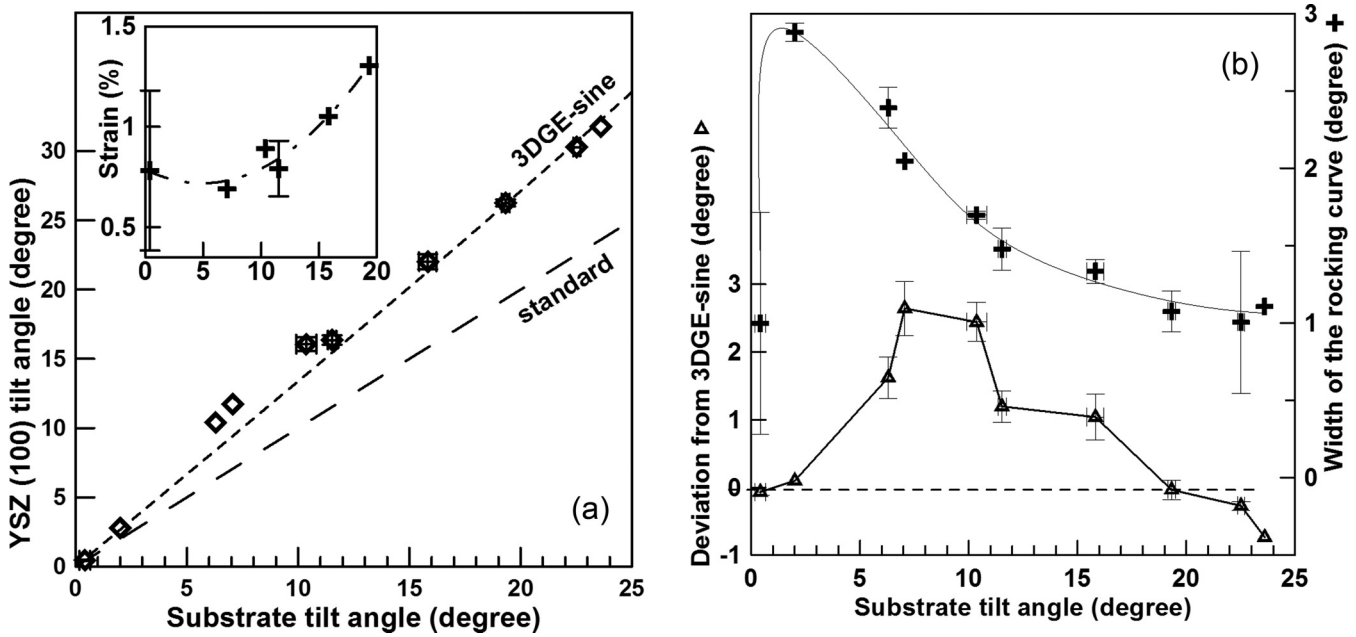

FIG. 6. Orientational relations of YSZ films on TAS NGO. (a) The film orientation follows the 3DGE-sine growth mode [Eq. (2)] at high substrate tilt angles and slightly exceeds the calculated value for 5°–12°. Inset: Dependence of the strain in the film on the substrate tilt angle. (b) Deviation from calculated tilt angle (3DGE-sine model, triangles) shows maximum in the 7°–10° range, correlating with the width of the rocking curve dependence on tilt angle (crosses). Lines are given as guides for the eye.

7°–10° [Fig. 6(b), bottom curve], but similarly decreases with tilt angle, finally changing to negative values for tilt angles above 20°. The FWHM of the rocking curve for the YSZ films deposited at tilt angles close to zero shows a very high spread from sample to sample [Fig. 6(b), top curve]. A change of the substrate tilt angle to ∼2° results in a huge rise of the grains misorientation (the FWHM increases to ∼3°). The further increase of the substrate tilt angle results in a gradual decrease of FWHM with saturation at ∼1° at high tilt angles.

The variation of the lattice parameter $\Delta d/d$ also shows a very high spread from sample to sample at zero tilt angle [see inset Fig. 6(a)]. Until 12° it remains almost constant, and increases only above 15°, when the deviation from the calculated angle becomes small and the width of the rocking curve saturates [Fig. 6(b)]. The strain and the width of the rocking curve show clear anticorrelation.

The lattice constant of the YSZ films varied from 5.134 to 5.157 Å (5.148 Å average, the measurement accuracy was low, ∼0.007 Å), independently on the substrate tilt angle. The deposition of YSZ films seem to be rather reproducible, no significant changes in film orientation and structure could be observed with small changes of deposition conditions. An increase of thickness of the YSZ film (100 to 900 Å) leads to a decrease of strain and a decrease of the rocking curve width: with an increase of film thickness the film becomes more homogeneous and more aligned.

3. $BaZrO_3$ *on NGO TAS*

The expected growth mode of a perovskite BZO film on a perovskite NGO substrate was standard, and for high (24°) tilt angles this assumption proved to be correct. Surprisingly, at a substrate tilt angle of 10° the film orientation showed excellent agreement with the geometrical model (Fig. 7). The discrepancy from the calculated value (tangent model) is less than 0.05°, and deviation from the standard orientational relations exceeds 0.8°. The width of the rocking curve increased for high tilt angle (see inset Fig. 7), similarly to the CeO_2 3DGE films [Fig. 4(b)]. The strain in the films decreased with tilt angle, anticorrelating to the rocking curve width. The measured lattice constant was 4.199 Å, in good agreement with the standard 4.2 Å value, and did not depend on tilt angle.

C. 3DGE growth in multilayer heterostructures

All studied multilayer heterostructures on NGO TAS showed 3DGE growth through the whole thickness of the heterostructure, except when a chemical reaction took place between the neighboring layers (YBCO over CeO_2, YSZ, or BZO). Even in these cases some part of the upper layer showed 3DGE growth, especially at lowered deposition temperatures.

1. $CeO_2/YSZ/NGO$

A thin (20–100 Å) CeO_2 layer is often introduced between the YSZ bottom layer and YBCO top layer to prevent chemical interaction. A weak signal from the thin CeO_2 layer is hard to distinguish from a strong neighboring YSZ peak, especially at small tilt angles. Still for some samples we managed to determine the mutual orientation of the films in

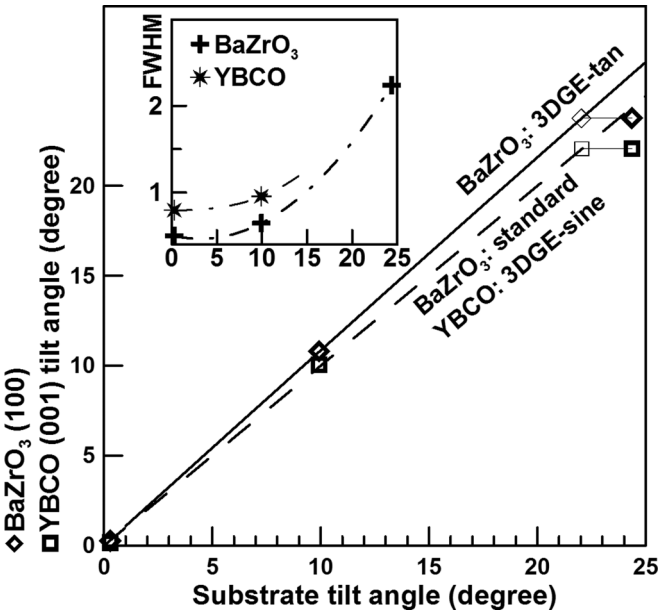

FIG. 7. Orientational relations in the YBCO/BZO heterostructures on TAS NGO. Diamonds: BZO, squares: 3DGE part of the YBCO films. Thin symbols: Calculated positions if BZO kept 3DGE growth mode to 24°. Inset: Dependence of the width of the rocking curve of the BZO (200) peak (crosses) and YBCO (005) peak (stars) on the substrate tilt angle. The lines on the inset are guides for the eye.

a YBCO/CeO_2(75 Å)/YSZ trilayer on NGO TAS (Fig. 8). We expected standard epitaxial growth of a fluorite CeO_2 film over a fluorite YSZ bottom layer, with strictly parallel (100) planes in both layers. Instead, the 3DGE growth was observed not only for the fluorite YSZ layer over the perovskite NGO substrate, but also for the CeO_2 film over the heterostructure (Fig. 8). The tilt angle for the CeO_2 layer is higher than that of the YSZ layer, in agreement with greater lattice constant (5.4

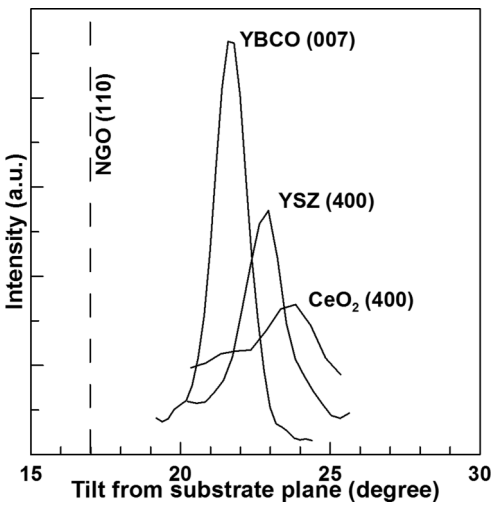

FIG. 8. Rocking curves of the (400) YSZ, (400) CeO_2, and (007) YBCO peaks of the trilayer YBCO/CeO_2/YSZ heterostructure on TAS NGO. The substrate tilt angle is 16.9°. All layers follow the 3DGE growth mode.

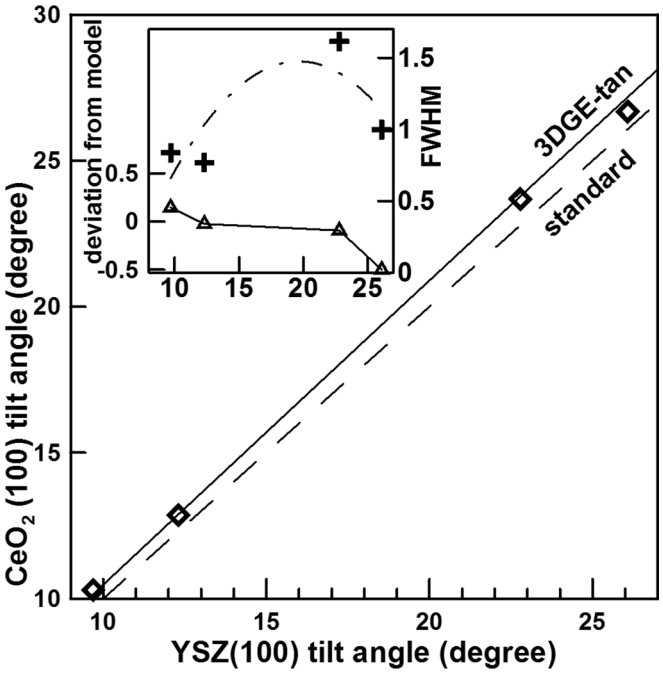

FIG. 9. Orientation of CeO_2 films on 3DGE YSZ layers on TAS NGO. Inset: Dependence of the deviation from the 3DGE-tangent model (triangles) and the width of the rocking curve of the CeO_2 (400) peak (crosses) on the substrate tilt angle. The lines are guides for the eye.

and 5.15 Å). The calculated and measured tilt angles match well (Fig. 9). The tangent model (1) describes the angular behavior better than the sine model (2), calculations are done taking into account an excessive tilt of the YSZ layer for tilt angles 5°–12° [Fig. 6(a)]. Similar to the CeO_2 films on bare NGO TAS the deviation from calculated value changes from positive to negative at ∼12° tilt of the underlaying layer [compare Fig. 4(b) and inset Fig. 9]. At high tilts (above 23° for CeO_2/YSZ) a deviation towards the standard growth mode is observed [Figs. 9 and 4(a)]. The width of the rocking curve increases with tilt angle, but drops when the tilt changes towards the standard orientation. We may conclude that all orientational features of the 3DGE tangent mode growth of CeO_2 on TAS NGO are preserved on tilted-axes YSZ bottom layer.

The measured lattice constant of the CeO_2 interlayer is 5.397 ± 0.009 Å, somewhat smaller than the standard 5.4 Å value, or 5.404 ± 0.004 Å typical for CeO_2 grown on NGO TAS at the same deposition conditions. Incorporation of Zr atoms into the CeO_2 growing film may be the reason for this difference.

2. *YBCO/CeO₂/NGO*

The YBCO grains on a CeO_2 layer showed either *c* orientation or 3DGE orientation; films with mixed orientation were observed most commonly. The orientation of the YBCO grains depended on tilt angle and deposition conditions, but the most affecting factors are the properties of the underlaying CeO_2 layer, set by CeO_2 fabrication technique, and preparation of the CeO_2/NGO sample to the YBCO film deposition.

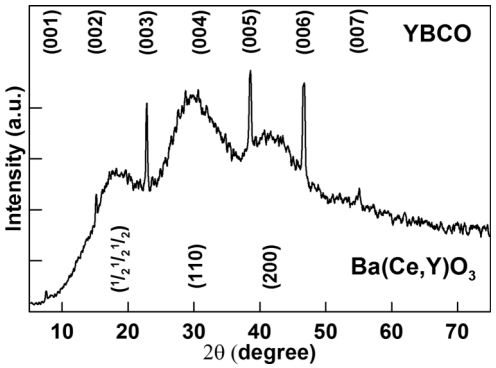

FIG. 10. X-ray $\theta/2\theta$ scan of the YBCO/CeO_2/NGO heterostructure along the substrate normal, nominal substrate tilt angle 22°. A set of broad peaks from polycrystalline Ba(Ce, Y)O_3 reaction layer can be detected on the scans, produced by small (5–15 Å) crystallites.

The mechanisms of *c*-oriented YBCO film formation over the CeO_2 layer are similar to the growth processes of YBCO films on the YSZ layers (see, e.g., [28,29]) and result from interaction of Ba with CeO_2 with formation of a Ba(Ce, Y)O_3 interlayer. An increase of thickness of such an interlayer leads to secondary seeding of Ba(Ce, Y)O_3 grains with orientations providing minimization of the surface energy. We observed (100), (110), and (111) orientations of Ba(Ce, Y)O_3 grains along the substrate plane (Fig. 10). The wide peaks in the angular range 10°–50° corresponded to very small (5–20 Å) crystallites with lattice constant ∼4.31 Å. The YBCO films on the Ba(Ce, Y)O_3 interlayer always showed *c*-oriented growth (Fig. 10), sometimes mixed with the tilted grains.

The tilt angle of the tilted YBCO grains differed both from the substrate tilt angle and the tilt angle of the 3DGE CeO_2 layer (Fig. 8), and increased monotonously with the substrate tilt angle, implying the 3DGE or some similar growth mechanism [Fig. 11(a), solid diamonds]. This effect was noticed in [21], but no explanation was suggested. Assuming 3DGE growth with a step height equal to $c/3 = 3.933$ Å (on the early stages of YBCO growth it tends to grow in the pseudocubic form), we get the YBCO tilt angle very close to that of the substrate (step height 3.864 Å), with a deviation below 1° in the whole possible range of tilt angles. The actual deviation from the substrate tilt angle is much higher [Fig. 11(a)].

The explanation for the 3DGE growth with the observed angles is also chemical interaction with formation of a very thin (not detected with XRD techniques) Ba(Ce, Y)O_3 layer between CeO_2 and YBCO films. This layer is strictly aligned with the underlying CeO_2 film, (100) Ba(Ce, Y) O_3||(100) CeO_2, and the tilt angle of the YBCO film is determined not by step height of CeO_2 layer but that of Ba(Ce, Y)O_3. From the atomistic point of view we may assume chemical bonding of the surface CeO layer with the incoming Ba atoms, with formation of a half of a perovskite $BaCeO_3$ cell, providing out-of-plane lattice constant (and, consequently, terrace step height) corresponding to $BaCeO_3$, not CeO_2. We note that 1/2- or 1/3-lattice constant as the height of the surface step was already mentioned before [15,17]. The agreement with the 3DGE-sine model assuming $BaCeO_3$ step height (4.31 Å measured for small crystallites)

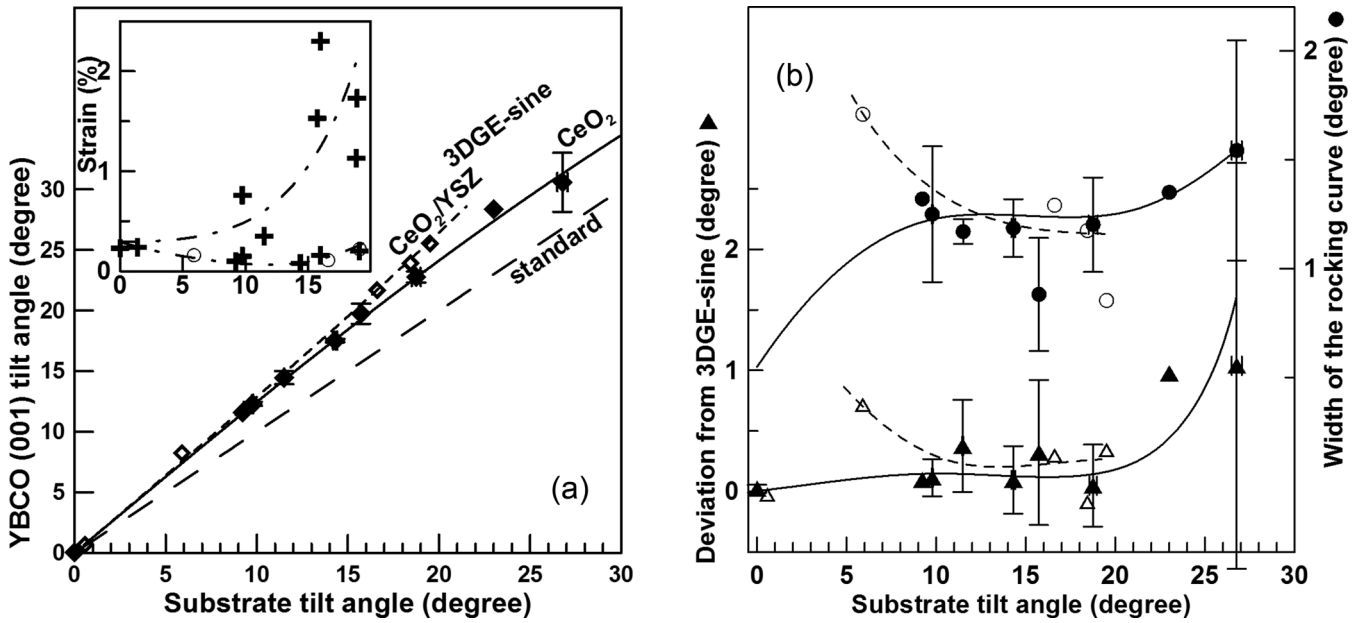

FIG. 11. Orientational relations of YBCO films on CeO_2 layers and on CeO_2/YSZ bilayers on TAS NGO. (a) The YBCO film orientation follows the 3DGE-sine growth mode [Eq. (2)] both for films grown on a single CeO_2 layer (solid diamonds, solid line) and on CeO_2/YSZ bilayers (open diamonds, short-dashed line). Inset: Dependence of the strain in the YBCO film on the substrate tilt angle, crosses: single CeO_2 layers, circles: CeO_2/YSZ bilayers. (b) Absolute deviation from calculated tilt angle (3DGE-sine model, triangles) correlates with the width of the rocking curve (circles). Solid symbols correspond to the YBCO films on single CeO_2 layers, open symbols YBCO films on CeO_2/YSZ bilayers. The lines are given as guides for the eye.

is impressive up to 27° [Fig. 11(a), solid diamonds]. Note that down-bending of the calculated dependence [solid line Fig. 11(a)] is determined by the tangent dependence of the tilt of the CeO_2 layer [Fig. 4(a)]. Measured data for the CeO_2 films at substrate tilt angles above 23° are absent, so the curve Fig. 11(a) in this range was calculated assuming tangent dependence for CeO_2 and sine formula for YBCO over the intermittent Ba(Ce, Y)O_3 layer.

The average deviation of the YBCO film orientation from the calculated value remained small (∼0.2°) until ∼20°, and rapidly increased for tilt angles above 20° [Fig. 11(b), solid triangles]. The FWHM of the rocking curves repeated this dependence [Fig. 11(b), solid circles]. The lattice constant c of the YBCO films was almost constant 11.684 ± 0.007 Å for all tilt angles below 20°. Precise determination of the lattice constants for higher angles was complicated due to the limitations of the applied asymmetric geometry of the x-ray diffraction. The strain $\Delta d/d$ was estimated for the same angular range 0°–20°; the films can be divided into two groups, with very low strain below 0.2%, and with strain increasing with tilt angle to 1% and more [see inset Fig. 11(a)]. The increasing dependence resembles strain behavior in the 3DGE YSZ films on TAS NGO.

3. *YBCO/CeO₂/YSZ/NGO*

The trilayer YBCO/CeO_2/YSZ structures were not studied extensively due to the low (30–80 Å) thickness chosen for the CeO_2 layers for the planned experiment. Still some samples allowed measurements for all three layers (Figs. 8 and 9).

The YBCO films on the CeO_2/YSZ bilayer show the same orientational behavior as on the single CeO_2 layers: c-oriented, 3DGE-oriented, and mixed-orientation films were formed depending on conditions for the chemical reaction with formation of a Ba(Ce, Y)O_3 layer. The properties of the 3DGE grains are shown with open symbols in Fig. 11.

The tilt of the YBCO film [Fig. 11(a), open diamonds] is described by the same sine model as in the bilayer case. Introduction of the YSZ layer with sine 3DGE dependence below a CeO_2 layer with tangent dependence results in a significant difference (0.3°–1.0°) between the measured values in the high-angle range, clearly distinguished with the applied XRD techniques. The deviation from the calculated value is slightly higher than for the YBCO 3DGE films on a single CeO_2 layer [Fig. 11(b), open triangles], and increases at low tilt angles (5°–8°). Unfortunately, there is no available data for YBCO 3DGE films on a single layer for this angular range. The YSZ 3DGE films showed a similar increase of deviation for the 5°–10° range [Fig. 6(b)]. The width of the rocking curve correlated well with the absolute deviation value, similarly to the YBCO 3DGE films on a single CeO_2 layer [Fig. 11(b), closed symbols]. The FWHM of the rocking curve in the angular range 15°–20° does not differ much from the measured values for YBCO 3DGE films on a single CeO_2 layer.

The lattice constant of the 3DGE YBCO films on the CeO_2/YSZ bilayers is the same as for the 3DGE YBCO films on single CeO_2 layers: 11.684 ± 0.005 Å, and also shows no angular dependence. The evaluated strain is low for all studied films, less than 0.25%, so all the YBCO films on bilayers belong to the low-strain group of samples [see inset Fig. 11(a)].

4. *YBCO/BaZrO$_3$/NGO and YBCO/BaZrO$_3$/YSZ/NGO*

To prove YBCO growth mechanisms on $BaCeO_3$ we fabricated a set of samples on TAS NGO with a 80-nm-thick buffer layer of $BaZrO_3$ from an available commercial target. The mechanisms of growth of *c*-oriented YBCO films on ZrO_2 are very similar to the growth of *c*-oriented YBCO on CeO_2, so we expected similarity also in case of 3DGE growth, if obtained on BZO.

The BZO films showed 3DGE behavior in the low-angle range 0°–10°, and a change to standard growth mode for high substrate tilt angle (24°, Fig. 7 diamonds). The YBCO films were growing in mixed orientation, with a *c*-oriented main part (>90%) and a 3DGE minor part (Fig. 7, squares). The step height of YBCO during growth is close to the lattice constant of NGO, so we expected back-rotation of the YBCO (001) plane towards the substrate plane and almost coincidence with the substrate (110) plane. This is exactly what we observed in experiment: agreement between the calculated and the measured values is better than 0.2° (Fig. 7, squares). The breach of the 3DGE growth mode of BZO at high tilt angles did not affect the 3DGE-sine growth mode of YBCO on BZO: assuming a tilt angle of BZO resulting from the 3DGE growth (thin diamond, Fig. 7) we get a position of the YBCO (001) plane exactly at the position calculated using 3DGE-sine model (thin square, Fig. 7).

To model the process of YBCO growth on CeO_2 we deposited YBCO/BZO heterostructures *in situ* on a 3DGE YSZ film on 16° TAS NGO. The result completely confirmed our predictions: the tilted part of the YBCO film (20.26° tilt) followed the 3DGE-sine model, with tilt angle of the bottom layer equal to that of the YSZ film (∼22°), but with a step height equal to the lattice constant of BZO (4.2 Å). This means that at least part of the ∼22.5-nm-thick BZO layer grows on the 3DGE YSZ film in the standard mode, (100) BZO‖(100) YSZ. With the available equipment we could not detect these standard-oriented BZO grains on the rocking curves, being out of the scan range.

The main part of the YBCO/BZO heterostructure showed the same properties as YBCO/Ba(Ce, Y)O_3 layer on 3DGE CeO_2 films. The main part of the BZO layer was growing (100), (110), and (111) oriented, with *c*-oriented YBCO growing over these grains. Some part of the BZO layer followed the 3DGE-sine growth mode on tilted YSZ layer with tilt angle of 19.28° (calculated value 19.35°). YBCO growth on these 3DGE BZO grains was not detected, neither in standard nor in 3DGE orientation.

IV. DISCUSSION

The growth of films with significant tilt of SICP from habit planes of the tilted-axes substrate are usually considered as rare and, in some sense, exceptions from the general rule of standard growth mode. Our results show that, in fact, for all-metaloxide heterostructures the 3DGE growth mechanism is more common than standard, especially for the angular range below 20°.

A. Epitaxial issues

To start discussing the 3DGE growth mechanism we should first revert to the question of epitaxy. In the very beginning this term was used when the structure of the film repeated the structure of the substrate. Rigorously only the films of the same material as the substrate, but with different dopant or with different level of doping, may be considered *epitaxial*. This term sometimes was also used to describe heterostructures in which the material of the film had the same lattice structure as the substrate, and the lattice constants did not differ much. Later the term *epitaxy* was used when a strict relation could be established between crystallographic planes and directions of the film and crystallographic planes and directions of the substrate. These films were also known as *oriented* films. The orientational relations with the substrate for some of the oriented films were set by the atomic structure of the substrate surface, and this class of film inherited the name of epitaxial films, while the films for which some of the orientational relations are set by film surface retained the name of oriented films.

The films presented in this study show *no* parallelism between some SICPs in the film and in the substrate, only the tilt axis is bonding the film and substrate lattice in a strict way. At the same time, the general orientation of the film is set not by the *surface* of the film, but by the *microstructure* of the substrate surface. The changes of the microstructure, in particular, the distance between the edges of the terraces, result in a change of the film orientation, in agreement with a strict mathematical relation. From this point of view the films are epitaxial, not just oriented.

The term *graphoepitaxy*, if it had been suggested in the very beginning of the fabrication of epitaxial films, would have been considered as an oxymoron, something like a "dry liquid." The orientation of the graphoepitaxial films was set not by the atomic structure of the substrate, but by the macroscopic structures of the surface of the substrate. Actually, the first graphoepitaxial films were fabricated from a material with totally different crystal structure from the structure of the substrate, making application of the term of "epitaxy" in the strict meaning absolutely impossible. Still the term settled, and at the moment the "graphoepitaxial" oriented films are fabricated, discussed, and categorized in different types (see, for example [30]).

Our films are (i) oriented and (ii) this orientation is set by the surface features of the substrate, i.e., they can be considered as graphoepitaxial. At the same time, the surface features that set the orientational relations are determined by the crystal structure of the substrate, and this makes our films epitaxial in the modern meaning of the term. Thus, the films grown by the 3DGE mechanism are epitaxial and graphoepitaxial at the same time.

We would like to emphasize a third point: the bonding of the lattices of the film and the substrate is realized in three orthogonal directions: the tilt axis, the length of the terrace, and the out-of-plane lattice constants set the orientational relations in a unique way. Moreover, the translational distances in all three directions are important for the film orientation, as well as matching (and mismatching) of these distances in the film and the substrate. This makes the discussed growth mechanism *essentially* three dimensional, and justifies the proposed name "three-dimensional graphoepitaxial," 3DGE, mechanism.

B. Growth modes and models

Disregarding the complicated microstructural mechanisms of formation of tilt in the films on TAS [11–13], we may identify two simplified mechanisms of formation of the 3DGE films: the overgrowth mechanism [15], and the simultaneous seeding mechanism [16].

The first one suggests seeding of the film near the edge-terrace joints, and growth of these from the terrace edge. When the growing layer reaches the end of the terrace, it encounters a different height of the surface that it should overgrow, and accommodates this difference [Fig. 1(b)]. The resulting angle depends on the length of the terrace d_t and simple considerations result in the tangent model (1). This growth mode corresponds to the graphoepitaxy of cases 2 and 3 in Fig. 1(b) in [30].

The second simplified model implies simultaneous seeding of the film on neighboring "seeding knots" in the edge-terrace joints [Fig. 1(c)]. In this case orientation of the film is formed in the same way as for the standard growth mode, because the seeding knots mimic the atom position in the atom-on-atom epitaxial growth. The tilt angle of the film depends on the distance between the seeding knots d_s, and the resulting model follows a sine dependence (2).

The two models hardly can be distinguished at tilt angles below 10°, so previous studies never faced a necessity to choose between these two mechanisms.

The first model seems to be more probable for small tilt angles, because the lattice of the growing layer should settle well before overgrowth would change the tilt angle. The demand to "settle" the structure of the growing layer means that at high angles this mechanism is improbable. Assuming two unit cells as a smallest "settled" seed, we get the limit for the tangent mode growth:

$$\gamma_t < \arctan[c_s/(2a_f)], \tag{4}$$

where a_f is the film unit cell size along the growth direction.

For CeO_2 growth on NGO this formula gives $\gamma_t = 19.7°$, and, indeed, at angles above 20° the CeO_2 film deviates towards the standard growth mode [Fig. 4(a)]. CeO_2 deposition on YSZ formula (4) gives 25.5°, and the observed deviation starts at 24°–25° (Fig. 9). The change of the growth mechanism to standard for BZO on NGO at 24° (Fig. 7, diamonds) also may be a result of limited angular range of the tangent growth mode ($\gamma_t = 24.7°$). For YSZ on NGO the limiting angle is 20.6°, but we cannot see a distinct trend towards standard growth mode even for ~23.5°. Note that the sine model provides a better fit for 3DGE growth of YSZ. Similarly no pronounced deviation towards standard growth at high angles was observed for YBCO on CeO_2, another pair of materials better described by the sine formula (Fig. 11).

The second simplified mechanism, simultaneous seeding, to the contrary, is promoted by a small distance between the seeding knots, and would be favorable at high tilt angles. At small tilt angles the seeding would be more efficient for closer placed seeding knots, so, taking into account a certain spread of the distance d_s along the substrate surface, we may expect slightly higher average tilt angles compared to the calculated value. This is exactly what happens for YSZ on NGO (Fig. 6), and for YBCO on CeO_2 [Fig. 11(b), open triangles].

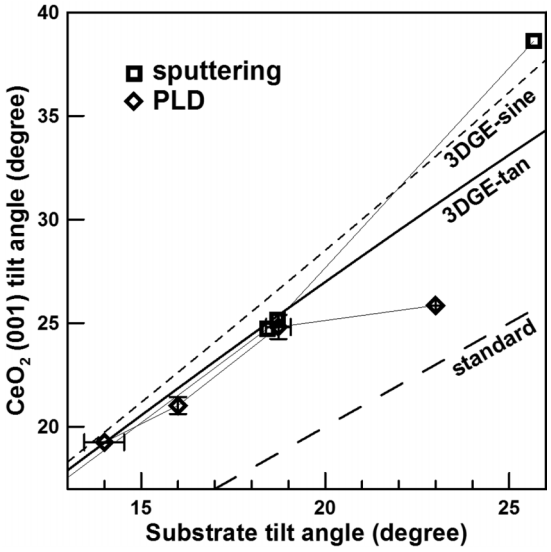

FIG. 12. Comparison of tilt of CeO_2 films on NGO TAS deposited by PLD (diamonds) and rf sputtering (squares, [19,20]) at high substrate tilt angles.

Do we really observe two different 3DGE growth modes, or is it just a measurement error? The data in Fig. 11(a) seem to prove the presence of two different modes: the YBCO films on a single CeO_2 layer and on a CeO_2/YSZ bilayer show different angular dependence in the range 15°–20° because a single CeO_2 layer fabricated by PLD follows the tangent mode, while a YSZ layer below CeO_2 demonstrates sine dependence. Comparison of CeO_2 films fabricated by different techniques also seem to prove the existence of two different growth modes (Fig. 12): the tilt of the PLD films at angles above 20° downturns towards the standard growth mode, while for the films deposited with sputtering techniques [19,20] the tilt still follows the 3DGE mechanism, sine dependence.

The data on growth modes for different film-substrate combinations are gathered in Table III. We could not unambiguously determine the factors that promote the overgrowth mechanism or the simultaneous seeding mechanism. Still, as much as we may conclude from the data in Table III, the compressive strain promotes the overgrowth mechanism, while films with tensile strain introduced by the underlying layer tend to follow the simultaneous seeding mode. Compressive strain, in the case of cubic film and substrate lattices, and equality of step height and lattice constant, corresponds to $c_f > c_s$ and increased tilt angle of the top layer compared to the tilt angle of the bottom layer. Tensile strain, with the same assumptions, corresponds to a decreased tilt angle of the top layer, so the tangent mode seems to be typical for the increase of the tilt angle due to the 3DGE growth mechanism, while the sine mode for the decrease of the tilt angle. This is not so for more complicated film-substrate matching, like YSZ/NGO, when tensile strain (and simultaneous seeding mechanism) is introduced into the film due to the 45° axes tilt in the habit plane (110) NGO, but the film tilt angle γ' increases because the step height of YSZ is higher than that of NGO (Fig. 6).

The dependencies of the critical parameters on the lattice mismatch seem to confirm this observation: for example,

TABLE III. Observation of sine and tangent growth modes for different film-substrate combinations.

Film/substrate	Lattice mismatch[a] (%)	Growth mode	γ_t, measured/calculated (deg)	Excessive tilt, value/range (deg)	Comment
BZO/NGO	-8.7– -8.8	tangent[b]	(<24)/24.7	n/a	
CeO_2/YSZ	-5.0	tangent	~24.5/25.5	n/a	
CeO_2/NGO	$+1.0$– $+1.1$	tangent	20/19.7	n/a	by PLD
		sine	n/a	no data	by rf sputtering
YBCO/CeO_2	-1.8– -0.1	sine	n/a	0.7/6	
YSZ/NGO	$+5.7$– $+5.8$	sine	n/a	2.5/(6–10)	
YBCO/BZO	$+7.4$– $+8.9$	sine[b]	n/a	(0.03/10)	
Ba(Y, Zr) O_3/YSZ	$+11.5$[c]	sine[b]	n/a	no data	

[a]Positive value corresponds to tensile strain, negative to compressive strain.
[b]Insufficient data for a reliable conclusion.
[c]No 45° in-plane rotation.

the deviation towards the standard mode for the overgrowth mechanism seems to start at smaller angles for higher compressive strain, as seen from the BZO/NGO, CeO_2/YSZ, and the CeO_2/NGO pairs. The excessive tilt at small tilt angles seems to increase with an increase of the tensile lattice mismatch, when we compare the YBCO/CeO_2 and YSZ/NGO combinations (Table III).

Two rows of Table III with small mismatches ~1% contradict to this suggested rule: YBCO/CeO_2 (small compressive strain, sine dependence) and CeO_2/NGO (small tensile strain, tangent dependence). If we suppose that the CeO_2 lattice constant is ~1.5% higher than measured, we remove this discrepancy: the lattice mismatch for CeO_2/NGO becomes weakly compressive (~ -0.5%), and for YBCO/CeO_2, weakly tensile (~ $+0.6\%$), in good agreement with the other data. The thermal expansion coefficients cannot account for such corrections, being almost the same for all three materials [NGO : $(4.5\text{–}9.0) \times 10^{-6}\,\mathrm{K}^{-1}$ from different references, CeO_2 : $(8.5\text{–}9.5) \times 10^{-6}\,\mathrm{K}^{-1}$, and YBCO : $(11\text{–}13) \times 10^{-6}\,\mathrm{K}^{-1}$]. The increase of the CeO_2 lattice constant during deposition can happen as a result of incomplete oxygenation (see discussion of oxygen removal from and incorporation to, for example, in [31]), and 1.5% is not the highest possible expansion. The missing oxygen could be incorporated into the CeO_2 layer immediately after the deposition, shrinking the lattice constant to the observed value.

For CeO_2/NGO both mechanisms were observed for different deposition techniques. We note that for e-beam evaporation and rf sputtering the deposition rate is small, so the CeO_2 film grows completely oxygenated, while for PLD a certain amount of oxygen vacancies is generated in the growing film, expanding the CeO_2 lattice. Tensile strain for the completely oxygenated CeO_2 films would account for sine mode for the e-beam evaporated and rf-sputtered films, while an increase of lattice constant by more than 1% during PLD would result in a compressive strain and tangent growth mode.

C. Orientational features

The width of the rocking curve is a parameter that sheds light on the peculiarities of the 3DGE film formation. The misorientation of the grains strongly depends on the seeding mechanism, and differences in rocking curve width dependence on angle imply formation of 3DGE films in different ways.

A comparison of properties of CeO_2 films on NGO TAS [Fig. 4(b)] and on YSZ 3DGE layers on NGO TAS (inset Fig. 9) show clear similarities. The deviation from the calculated curve slowly decreases from small-positive to small-negative values until the threshold angle γ_t, when negative deviation rapidly increases. This dependence is accompanied by an increase of the width of the rocking curve until the same threshold angle, after which it drops to smaller level. Both sets of data can be brought to the same scale by plotting the dependence on the film tilt angle instead of using the substrate tilt angle, and by normalizing the deviation from the calculated value by division on the inclination $(\gamma' - \gamma)$ due to the 3DGE growth mechanism. This transformation makes visible the identity of the two dependencies [Fig. 13(a)]. Unfortunately, we have not enough data in the range 0°–10° to present the complete dependence of the deviation from the geometrical model (1).

The reasons for the misorientation of the grains of the film were presented in [15]. The terraces on the substrate surface are not equal, so a certain spread of the orientation of the grains after overgrowth of the next step is present from the beginning, and strongly depends on the size of the grains of the film. If the grains are smaller than the typical terrace length d_t, the grains would grow following the standard growth mode. This effect is clearly demonstrated in [17], where the change of the growth mode to standard at low deposition temperature is a result of a decrease of the size of the CeO_2 grains. The combination of a distribution of size of the grains and a distribution of the length of the terraces results in a distribution of the orientation of the grains starting from the standard mode and until film tilt angles exceeds the calculated γ_t using the geometrical model. The spread of the orientation of the grains will increase when step bunching starts on the substrate surface, with formation of steps with height 2, 3, and more times the ordinary height c_s. For the typical perovskite substrates step bunching starts at ~10°, depending on preparation conditions [5], and we observe an increase of the width of the rocking curve at ~13° [Fig. 13(a)]. The rapid decrease of the film tilt angle towards the standard relations at angles above the threshold γ_t may be a result of very small lengths of terraces, so that the overgrowth happens

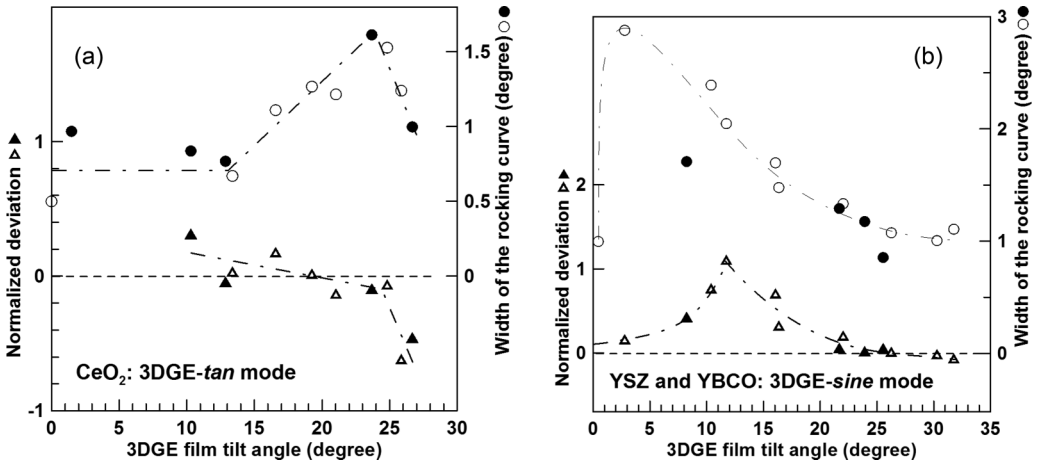

FIG. 13. Orientational properties of the 3DGE films with different growth mechanism. The overgrowth mechanism (a) shows an increase of the rocking curve width accompanied by a slow decrease of the deviation from positive to negative values until after the threshold angle FWHM of rocking curve decreases and the negative deviation rapidly increases. Open symbols: CeO_2 films on NGO TAS, solid symbols: CeO_2 films on 3DGE YSZ film on NGO TAS. The simultaneous seeding mechanism (b) shows a gradual decrease of width of the rocking curve from very high level obtained at very low tilt angles. The deviation shows a peak at $\sim 12^\circ$. Note that the YBCO films (solid symbols) were deposited over a YSZ layer (with a CeO_2 interlayer), so the observed agreement between YBCO and YSZ (open symbols) data may be explained as inheritance of the properties of the bottom layer. The lines are given as guides for the eye.

over two or more steps and the geometrical model (1) becomes invalid.

The dependencies for the sine model are completely different [Fig. 13(b)]. Even a small tilt of the substrate SICPs results in a very broad rocking curve of the film. A very high spread of the width of the rocking curve of the YSZ films on a standard-oriented substrate [Fig. 6(b)] implies realization of the 3DGE-sine mechanism even at very low tilt angles that are always present on the surface of a standard-oriented substrate due to inhomogeneous polishing. The rocking curves become more and more narrow with an increase of the substrate tilt until the FWHM of the rocking curves saturates at $\sim 20^\circ$ (film tilt angle $\sim 25^\circ$). The deviation from the calculated value at this angle changes from positive to negative, but remains small—no turn-down to the standard epitaxial relations was observed for the 3DGE-sine growth mode in the whole studied range, until $\sim 35^\circ$. The highest deviation is observed at 5°–10° [film tilt $\sim 12^\circ$, Fig. 13(b)]. This dependence is well explained by the simultaneous seeding mechanism. At high tilt angles the seeding knots on the substrate surface form a dense network, providing good conditions for seeding of the grains with the exact tilt angle, determined by condition (2). Both deviation and misorientation of the grains is small. A decrease of the substrate tilt angle increases the distances between the seeding knots and, hence, increases the width of the distribution of d_s. An immediate consequence is the increased misorientation of the grains of the film and, hence, the width of the rocking curve. This tendency remains the same until very small angles, when the standard growth mode becomes dominant. Another consequence of the increased distance between the seeding knots is a shift of the distribution of the orientation of the grains towards higher tilt angles. The reason is a higher probability of seeding of a grain of a certain orientation when the distance between the seeding knots is smaller, i.e., with higher tilt angle. This effect is less influential when all distances d_s become long and the probability of seeding becomes even. For the YSZ films this happens for substrate tilt angles below 7° (film tilt angle $\sim 12^\circ$).

YBCO on CeO_2 seems to grow in the 3DGE-sine mode also (Fig. 11), but we could not observe the same effects as for YSZ. The probable reason is the inheritance of the tangent mode properties of the CeO_2 layer. The YBCO films on a CeO_2/YSZ bilayer shows dependencies similar to that of YSZ [solid symbols in Fig. 13(b)] but, again, it may be a consequence of the sine growth mode of the YSZ layer below. The parameters of the YBCO films on a CeO_2/YSZ bilayer after normalization lies along the same lines as that of YSZ 3DGE films [Fig. 13(b)].

An excess of film tilt (0.5°–1°) over the calculated using the geometrical model was observed for CeO_2 on Ni in [17]. The angular range for this excessive tilt increased with deposition temperature T_D from 1°–11° at 785 °C, to 1°–15° at 700 °C, and 2°–15° at 600 °C (the upper angular limit for the excessive tilt is observed only for the highest T_D). Assuming simultaneous seeding over a step, we get higher probability of seeding on long distances d_s with increased T_D, and, hence, a shift of the excessive tilt range to smaller tilt angles.

D. Effect of surface features

The 3DGE growth mechanism essentially depends on the morphology of the substrate. Rigorous preparation of the substrate surface by chemical etching and annealing at high temperature (surface reconstruction) results in a regular sequence of uniform steps one-unit-cell high. Such a substrate provides the most refined conditions for testing certain growth effects and mechanisms.

Unfortunately, our depositions were performed on the substrates with no special treatment to form the SICP-faceted growth steps. The substrate showed a very smooth surface,

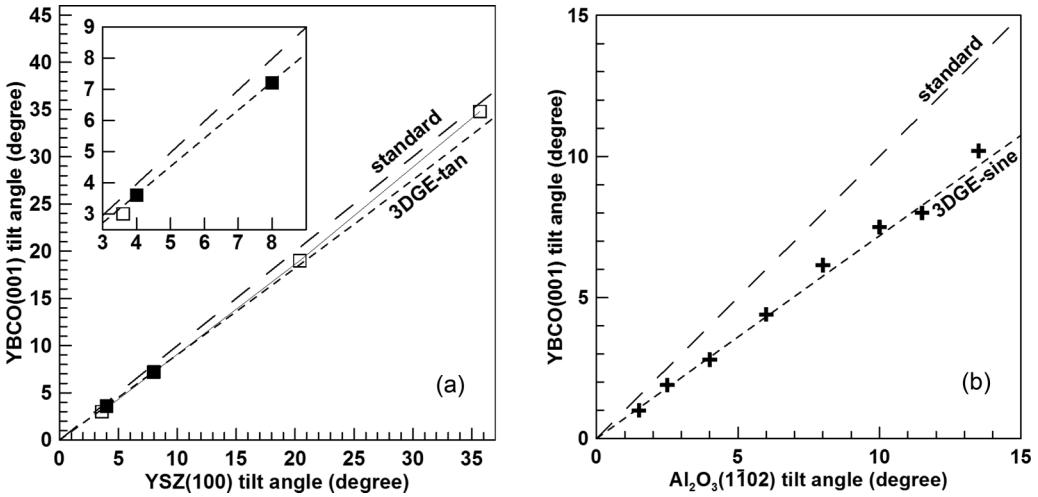

FIG. 14. Examples of 3DGE growth in studies of other groups. (a) YBCO deposition over YSZ TAS with (open squares, [23]) and without (solid squares, [22]) Y_2O_3 buffer layer. (b) YBCO deposition over CeO_2 layer on sapphire TAS [22]. Note that Y_2O_3 over YSZ and CeO_2 over sapphire grow in the standard mode.

with roughness R_a less than 2 Å, with no oriented or elongated features even for the TAS with high tilt angle. Observation of such a morphology implies the presence of damaged "amorphous" areas at least on some part of the substrate surface. Applicability of the geometrical growth mechanisms [Figs. 1(b) and 1(c)] was under serious doubts. Still the 3DGE growth mechanism was reliably detected for the majority of the tested top layer/bottom layer combinations. We may conclude, that even substrates that were not undergoing the surface reconstruction procedure provide good enough conditions for realization of the 3DGE growth. In fact, the 3DGE mechanism was *not* observed only when the bonds between film and bottom layer were broken by intense chemical interaction (YBCO on YSZ, and, for some deposition conditions, on CeO_2 and BZO), and when the film and substrate were of the same crystal structure and the lattice mismatch between them was small ∼1% (YBCO on NGO).

Considering the effect of the surface morphology on the formation of the 3DGE films, we notice that even after severe step bunching (5° tilted from (0001) plane sapphire substrates after annealing at 1500 °C showed steps ∼40 Å high [15]) the substrates provided good enough conditions for the 3DGE growth, i.e., both damaged amorphous surfaces and high steps after step bunching still allow growth by the 3DGE mode, implying a very high tolerance of this growth mode to the surface conditions.

One more important issue referring to the substrate surface preparation is the orientation of the tilt axis. In our experiments the tilt axis was quite close to the [001] axis of the substrate, providing good conditions for "initial" matching of the film and substrate lattices. We cannot confidently claim that the film orientation will follow the 3DGE growth mode if the tilt axis is chosen along some other crystallographic direction. It is known that the change of the orientation of the surface features can influence orientation of the growing films (see, e.g., [32–34]). Experiments in semiconductor heterostructures showed a broad variety of effects of changing the tilt axis direction in the habit plane. Already in [8] the 3DGE growth mode of Ga(In)As was observed along the ⟨−110⟩ direction on the GaAs (001) plane, but not along orthogonal ⟨110⟩ direction. In [11] CdS_2 growth on sapphire showed 3DGE growth for all orientations of the tilt axis, while Si on sapphire, similarly to [8], showed the 3DGE behavior for tilt along only one of two orthogonal directions. The reason was different surface morphology resulting from miscut in nonsymmetric crystallographic directions [11]. The most complicated film tilt mechanism was observed in [35], when misfit level changed not only the film tilt angle, but also direction of tilt as seen from the habit plane. Ni grains orientations in [17] were "randomly" distributed along a predominant orientation, so the tilt axes on different grains were randomly oriented in the habit plane. All CeO_2 grains showed the same 3DGE growth mode, implying completely isotropic behavior of ceria on Ni [17]. In our case changing the tilt axis to [111] (45° tilt from the [001] direction in the (110) habit plane of NGO) may result in 3DGE growth with the same relations along the habit plane, or 45° tilt of the film axes in habit plane, or in 45° tilt of the film axes normal to the habit plane—all these initial orientational relations are possible and should be checked experimentally for each pair top layer/bottom layer. We even cannot claim that the 3DGE mechanism would be preserved if the tilt axis is changed.

E. Evidences of 3DGE growth in all-metaloxide heterostructures in the literature

In the Introduction part of this paper we mentioned some observations of the 3DGE growth mode by other groups. In fact, these observations are more numerous, but sometimes these data were misinterpreted or left without explanation.

In [22] two combinations film-substrate (YBCO/YSZ and $YBCO/CeO_2/Al_2O_3$) were studied in a wide angular range, 0°–14°, orientation of both is finely described by the 3DGE growth mechanism. YBCO grows over YSZ in the same way as YBCO over CeO_2 in our experiments, with formation of $Ba(Zr, Y)O_3$ interlayer aligned with the YSZ SICPs [Fig. 14(a), solid squares]. YBCO over CeO_2 follows the 3DGE-sine growth mode assuming no chemical

interaction between YBCO and CeO_2, but CeO_2 grows on sapphire according to the standard mode, with parallel SICPs : (001) CeO_2||(1 − 1 0 2) Al_2O_3 [Fig. 14(b)]. Actually, agreement with the 3DGE-tangent mode is marginally better, but we decided to keep the sine model in agreement with our results. Anyway, the difference between the sine and tangent modes in the 0°–14° range is less than 0.15°, being hardly distinguishable without special precautions during measurement. Note that a very good agreement is obtained using lattice constants for YBCO (11.685 Å), YSZ (5.149 Å), CeO_2 (5.405 Å), and Ba(Y, Zr) O_3 (4.31 Å), as measured in our experiments. No attempts to improve conformity by fitting the lattice constants was done.

Another example of 3DGE growth is presented in [23]. The YBCO films buffered by a Y_2O_3 layer on a YSZ TAS showed a pronounced tilt of the SICP from the habit plane of the substrate in the range 3°–36°. Again we get a good agreement between the presented numbers and calculated using formula (1), assuming chemical interaction with formation of Ba(Y, Zr)O_3 with the same orientation of the SICP as that of the substrate and buffer layer [Fig. 14(a), open squares]. A tendency towards standard growth mode is observed at high angles, similarly to our results with BZO deposition on NGO TAS (Fig. 7), so we used the tangent model for the calculation. The agreement with the geometrical model is less accurate compared to [22] results, either due to an unknown composition of the product of chemical interaction in the beginning of the YBCO film growth, or simply as a result of the approximate numbers given in [23].

Deposition of YBCO on YSZ layer in our experiments always resulted in *c*-oriented YBCO films, in contradiction with the results [22], where 3DGE growth started after initial chemical interaction with formation of Ba(Y, Zr)O_3 layer. Yttrium segregation on the YSZ substrate surface during substrate preparation may be the reason, forming a $Y(Zr)_2O_3$/YSZ surface layer similar to Y_2O_3/YSZ in [23]. Such segregation is expected at high oxygen partial pressure, during annealing of the substrates after CMP, or during the prebake step immediately before deposition [36].

Theis and Schlom [24] present a much more complicated heterostructure, where tetragonal $PbTiO_3$ grows on a $SrTiO_3$ TAS in two different orientations. Accurate modeling of the growth mode demands precise measurement of the lattice constants that are affected by stoichiometry and substrate-induced strain. Still the agreement with the geometrical model is more than qualitative. In [37] a significant distortion of the lattice should be taken into account to obtain agreement between the geometrical model and the observed data. Reference [35] also notes importance of possible tetragonal distortions introduced by the substrate. These experiments demonstrate that the good agreement between calculated and measured values in our experiments is, in some sense, a coincidence, at least when such materials as CeO_2 are considered. The structure of CeO_2 is easily distorted by the substrate-induced strain, and the lattice constant of ceria strongly depends on density of oxygen vacancies generated during deposition (see, e.g., [17,31,38]). Reasonable agreement of the experimental data with the simplified model (1) is, to some extent, a fortunate combination of circumstances, including oxygenation during and after deposition, and thickness of the films high enough to ignore the substrate-induced strain in the interface area.

The possible effect of lattice distortion can be illustrated with results of [18] [see Fig. 2(a)]. The critical angle γ_c, calculated using standard ceria lattice constant, is smaller than the observed one (30.4° and 32°, respectively). Taking into account tetragonal distortion of ceria by the substrate-introduced tensile strain [assuming volume-preserving distortion and strain introduction only along the habit plane (110) NGO], we obtain $\gamma_c = 31.2^\circ$, in better agreement with the measured value. In fact, such estimation should consider also the strain introduced by the edges of the steps on the substrate surface, a decrease of the unit cell volume in the strained lattice, and expansion of the lattice due to oxygen nonstoichiometry during deposition. All these factors are decreasing the calculated γ_c, so the accurate estimation would be in between 30.4° and 31.2°. For our CeO_2 films fabricated by PLD we do not observe a substantial tetragonal distortion. The ceria lattice constant measured along the normal to habit plane (110) NGO showed no dependence on angle and remained close to the value measured for the standard-oriented substrate. With increasing tilt angle the effect of mismatch with the habit plane is decreasing, and the counteracting strain introduced by the step edges is increasing. Constant lattice parameter, thus, means that the film grows independently on the substrate-induced strain and the lattice constant depends mainly on the deposition conditions (and corresponding density of oxygen vacancies in the film). An indirect proof of weak effect of tetragonal distortion for our films is a good match between the calculated and measured film tilt values (Fig. 4).

Hoek *et al.* [39] provide another example of a more complicated mechanism matching top and bottom layers. The SICPs of La(Sr)CuO_4 grown on a 26° ramp etched of Nd(Ce)CuO_4 demonstrated a 3.3° inclination to the SICPs of the bottom layer. The inclination monotonously changes with the tilt angle of the ramp. The geometry of growth and the behavior of the inclination are similar to that discussed in our study, but application of the simple geometrical model gives a smaller tilt angle of 2.8°. Authors [39] suggest a more sophisticated mechanism of matching of corresponding facets, say, (3 0 19), of the top and bottom layers during growth, with simultaneous matching of both in-plane and out-of-plane lattice constants. This approach provides excellent agreement with the observed tilt angle between the SICPs of two layers. Similar results can be obtained for twin boundaries [39], where facet matching is the obvious mechanism of strain accommodation on the grain boundaries. References [11] and [40] also point out matching at higher symmetries (symmetric [11] and asymmetric [40] boundaries) as an alternative to the simple geometrical matching at the film-substrate interface.

V. CONCLUSION

We studied growth by PLD of metaloxide thin films on $NdGaO_3$ substrates with the surface tilted from the standard (110) crystallographic plane. Eight of ten studied top layer/bottom layer combinations showed a growth mode resulting in an inclination between the SICPs of the top layer and the corresponding SICPs of the bottom layer. The observed dependence of top layer tilt angle on the tilt angle of

the bottom layer is well explained by a simple geometrical growth model, taking into account faceting of the surface of the bottom layer. The resulting growth mode depends both on standard atom-on-atom epitaxial matching along the tilt axis, graphoepitaxial matching in the normal to tilt axis direction in the substrate plane, and on the ratio of growth steps heights of the top and bottom layer, i.e., the matching of the top and the bottom layer is three dimensional. This growth mechanism may be described as a three-dimensional graphoepitaxial (3DGE) growth.

The 3DGE growth mechanism seems to be quite common for deposition on TAS with tilt angles more than 5°. PLD, rf sputtering [19,20], e-beam evaporation [18], and even LPE [15] provided conditions good enough for the 3DGE growth. No special substrate treatment is needed, even substrates with damaged amorphous surface or with step bunching [15] are suitable. The 3DGE growth mechanism is observed in multilayer structures, both when the bottom layer follows 3DGE mode and when it grows with standard epitaxial relations. The 3DGE growth was observed both with increase and decrease of the top layer tilt angle compared to the tilt angle of the bottom layer.

Two different 3DGE dependencies may be distinguished in the high-angle range (>15°): with a tendency towards standard growth above some threshold angle, and retaining 3DGE behavior until a tilt angle of 45° is reached, either by top or by bottom layer. The first type is better described by a tangent angular dependence, and usually is observed when a compressive strain is induced in the top layer. The second type follows a sine dependence, and is usually seen for tensile-strained top layers. An increase over the calculated value tilt is often observed in the range 5°–10° for the sine-type dependencies. In a simplified way the difference may be attributed to two different formation mechanisms, "overgrowth" and "simultaneous seeding." The first one forms the tilt different from the bottom layer when the growing grain overgrows another grain. For the second mechanism the top layer tilt is formed right when the grain is seeded. Some material combinations showed both dependencies, for different deposition conditions. The reasons for realization of each of these dependencies should be clarified.

The results presented in this paper were obtained for materials with a simple cubic lattice (or the lattice that can be reduced to a pseudocubic during growth at high deposition temperature). Reports from other groups point to the fact that a simple geometrical model of 3DGE growth may be of limited validity in cases of more complex lattices, when the top layer experiences significant distortions due to a bottom layer induced strain, or when the boundary between two layers exhibits mirror or central symmetry.

ACKNOWLEDGMENTS

The work was supported by Program of FASO of Russia. I.K.B. also wishes to acknowledge FCT for its financial support (Grant No. IF/00582/2015).

[1] C. Tegenkamp, J. Phys.: Condens. Matter **21**, 013002 (2009).
[2] M. Mukaida, Sh. Miyazawa, and M. Sasaura, Jpn. J. Appl. Phys. **30**, L1474 (1991).
[3] J. Brotz, H. Fuess, T. Haage, J. Zegenhagen, Ch. Jooss, A. Forkl, and R. Warthmann, J. Appl. Phys. **85**, 635 (1999).
[4] H. Song and T. S. Sudarshan, J. Cryst. Growth **371**, 94 (2013).
[5] J. Zegenhagen, T. Haage, and Q. D. Jiang, Appl. Phys. A **67**, 711 (1998).
[6] Ch. Chen, Zh. Chen, J. Zhang, and X.-J. Du, Sci. China Phys. Mech. Astron. **55**, 2042 (2012).
[7] O. Igarashi, J. Appl. Phys. **42**, 4035 (1971).
[8] H. Nagai, J. Appl. Phys. **45**, 3789 (1974).
[9] G. H. Olsen and R. T. Smith, Phys. Status Solidi A **31**, 739 (1975).
[10] O. Igarashi, Jpn. J. Appl. Phys. **15**, 1435 (1976).
[11] M. Aindow and R. C. Pond, Philos. Mag. A **63**, 667 (1991).
[12] F. Riesz, J. Appl. Phys. **79**, 4111 (1996).
[13] J. P. Hirth and R. C. Pond, Philos. Mag. **90**, 3129 (2010).
[14] A. Petkova, J. Wollschlaeger, H.-L. Guenter, and M. Henzler, Surf. Sci. **542**, 211 (2003).
[15] R. Bachelet, G. Nahelou, A. Boulle, R. Guinebretiere, and A. Dauger, Prog. Solid State Chem. **33**, 327 (2005).
[16] I. K. Bdikin, J. E. Mozhaeva, P. B. Mozhaev, C. S. Jacobsen, J. Bindslev Hansen, A. L. Kholkin, V. A. Luzanov, and I. M. Kotelyanskii, report on MATERIAIS 2005: XII Portuguese Materials Society Meeting, III International Materials Symposium, Aveiro, Portugal, 2005 (unpublished).
[17] J. D. Budai, W. Yang, N. Tamura, J.-S. Chung, J. Z. Tischler, B. C. Larson, G. E. Ice, Ch. Park, and D. P. Norton, Nat. Mater. **2**, 487 (2003).
[18] I. M. Kotelyanskii and V. A. Luzanov (private communication, 1996).
[19] I. K. Bdikin, P. B. Mozhaev, G. A. Ovsyannikov, F. V. Komissinskii, I. M. Kotelyanskii, and E. I. Raksha, Phys. Solid State **43**, 1611 (2001).
[20] I. K. Bdikin, P. B. Mozhaev, G. A. Ovsyannikov, P. V. Komissinski, and I. M. Kotelyanskii, Physica C **377**, 26 (2002).
[21] P. B. Mozhaev, J. E. Mozhaeva, I. K. Bdikin, I. M. Kotelyanskii, V. A. Lusanov, J. Bindslev Hansen, C. S. Jacobsen, and A. L. Kholkin, Physica C **434**, 105 (2006).
[22] E. Stepantsov, M. Tarasov, A. Kalabukhov, L. Kuzmin, and T. Claeson, J. Appl. Phys. **96**, 3357 (2004).
[23] C. H. Mueller, P. H. Holloway, J. D. Budai, F. A. Miranda, and K. B. Bhasin, J. Mater. Res. **10**, 810 (1995).
[24] C. D. Theis and D. G. Schlom, J. Mater. Res. **12**, 1297 (1997).
[25] S. Kim, Y. Kang, and S. Baik, Thin Solid Films **256**, 240 (1995).
[26] P. B. Mozhaev, A. V. Khoryushin, J. E. Mozhaeva, J.-C. Grivel, J. Bindslev Hansen, and C. S. Jacobsen, J. Supercond. Novel Magnetism **30**, 2401 (2017).
[27] P. B. Mozhaev, J. E. Mozhaeva, I. K. Bdikin, T. Donchev, E. Mateev, T. Nurgaliev, C. S. Jacobsen, J. Bindslev Hansen, S. A. Zhgoon, and A. E. Barinov, Proc. SPIE **5401**, Micro- and Nanoelectronics 2003 (2004).
[28] J. A. Alarco, G. Brorsson, Z. G. Ivanov, P.-A. Nilsson, E. Olsson, and M. Lofgren, Appl. Phys. Lett. **61**, 723 (1992).

[29] J.-H. Kim, S. Oh, and D. Youm, Thin Solid Films **305**, 304 (1997).
[30] E. I. Givargizov, Thin Solid Films **189**, 389 (1990).
[31] F. Wu, A. Pavlovska, D. J. Smith, R. J. Culbertson, B. J. Wilkens, and E. Bauer, Thin Solid Films **516**, 4908 (2008).
[32] G. Brorsson, E. Olsson, Z. G. Ivanov, E. A. Stepantsov, J. A. Alarco, Yu. Boikov, T. Claeson, P. Berastegui, V. Langer, and M. Loefgren, J. Appl. Phys. **75**, 7958 (1994).
[33] D. Vassiloyannis and P. M. Pardalos, Physica C **468**, 147 (2008).
[34] M. Sunder and P. D. Moran, J. Electron. Mater. **38**, 1931 (2009).
[35] A. Pesek, K. Hinger, F. Riesz, and K. Lischka, Semicond. Sci. Technol. **6**, 705 (1991).
[36] X.-G. Wang, Surf. Sci. **602**, L5 (2008).
[37] D. A. Neumann, H. Zabel, and H. Morkoc, J. Appl. Phys. **64**, 3024 (1988).
[38] D. P. Norton, C. Park, J. D. Budai, S. J. Pennycook, and C. Prouteau, Appl. Phys. Lett. **74**, 2134 (1999).
[39] M. Hoek, F. Coneri, N. Poccia, X. Renshaw Wang, X. Ke, G. Van Tendeloo, and H. Hilgenkamp, Appl. Phys. Lett. Mater. **3**, 086101 (2015).
[40] B. W. Dodson, D. R. Myers, A. K. Datye, V. S. Kaushik, D. L. Kendall, and B. Martinez-Tovar, Phys. Rev. Lett. **61**, 2681 (1988).